
INTERNATIONAL JOURNAL OF ENGINEERING RESEARCH AND INNOVATION

The INTERNATIONAL JOURNAL OF ENGINEERING RESEARCH AND INNOVATION (IJERI) is an independent and not-for-profit publication, which aims to provide the engineering community with a resource and forum for scholarly expression and reflection.

IJERI is published twice annually (fall and spring issues) and includes peer-reviewed research articles, editorials, and commentary that contribute to our understanding of the issues, problems, and research associated with engineering and related fields. The journal encourages the submission of manuscripts from private, public, and academic sectors. The views expressed are those of the authors and do not necessarily reflect the opinions of the IJERI editors.

EDITORIAL OFFICE:

Mark Rajai, Ph.D.
Editor-in-Chief
Office: (818) 677-2167
Email: ijmeeditor@iajc.org
Dept. of Manufacturing Systems
Engineering & Management
California State University-
Northridge
18111 Nordhoff Street
Northridge, CA 91330-8332

THE INTERNATIONAL JOURNAL OF ENGINEERING RESEARCH AND INNOVATION EDITORS

Editor-in-Chief:

Mark Rajai

California State University-Northridge

Associate Editors:

Paul Wilder

Vincennes University

Li Tan

Purdue University North Central

Production Editor:

Philip Weinsier

Bowling Green State University-Firelands

Subscription Editor:

Morteza Sadat-Hossieny

Northern Kentucky University

Web Administrator:

Saeed Namyar

Advanced Information Systems

Manuscript Editor:

Philip Weinsier

Bowling Green State University-Firelands

Copy Editors:

Li Tan

Purdue University North Central

Ahmad Sarfaraz

California State University-Northridge

Technical Editors:

Marilyn Dyrud

Oregon Institute of Technology

Michelle Brodke

Bowling Green State University-Firelands

Publisher:

Bowling Green State University Firelands

TABLE OF CONTENTS

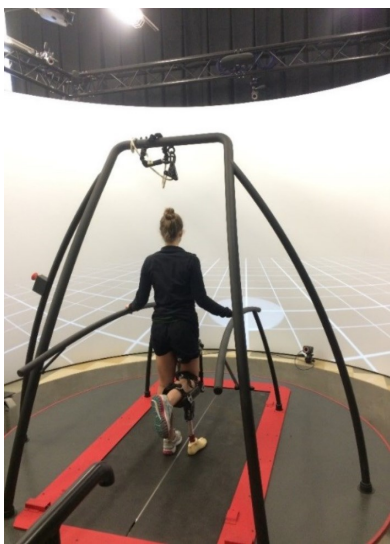
<i>Editor's Note (In This Issue): 3D Motion Tracking, Artificial Neural Networks, Wireless Control of a Robotic Arm</i>	3
Philip Weinsier, IJERI Manuscript Editor	
<i>The Implementation of Recycled Thermosetting Composite Powder in Rotational Casting</i>	5
Dru M. Wilson, Central Michigan University	
<i>Wireless Control of a Robotic Arm Using 3D Motion Tracking Sensors and Artificial Neural Networks</i>	13
Fernando Rios, Georgia Southern University; Rocío Alba-Flores, Georgia Southern University; Imani Augusma, Georgia Southern University	
<i>Comparative Study in the Optimal Design of Custom-Constructed Wind Augmentation Shrouds</i>	25
Ulan Dakeev, Texas A&M University-Kingsville; Farzin Heidari, Texas A&M University-Kingsville; Mohammad Mustaq Bijapur, Texas A&M University-Kingsville; Sumanth Yanamala, Texas A&M University-Kingsville	
<i>Thermal Performance of Recycled Aggregate Using Building Energy Simulation Programs</i>	30
Thomas Nicholas, The University of North Carolina at Charlotte; Tara Cavalline, The University of North Carolina at Charlotte; Dixie Johnson, The University of North Carolina at Charlotte; Morgan Laney, The University of North Carolina at Charlotte	
<i>Concrete with Enhanced Ductility Using Structural Microfibers</i>	40
Shane M. Palmquist, Western Kentucky University; Ramyasree Annam, Western Kentucky University	
<i>Instructions for Authors: Manuscript Submission Guidelines and Requirements</i>	45

IN THIS ISSUE (P.13)

3D MOTION TRACKING, ARTIFICIAL NEURAL NETWORKS, WIRELESS CONTROL OF A ROBOTIC ARM

Philip Weinsier, IJERI Manuscript Editor

One of the great things about being the editor of these journals is reading about all of the exciting research that our authors engage in. And while I hope to entice you, with these “*In This Issue*” pieces, to read the related articles published in the respective issues, I also want to expand the perspective to related devices or activities that are already part of our world. The authors of the article in this issue developed both the hardware and software components for an intelligent system that is able to wirelessly control the movements of a robotic arm for mimicking gestures of a human arm. Their work included 3D wireless motion tracking sensors, a microcontroller to drive the six-degree-of-freedom (6DOF) robotic arm, and the training of an artificial neural network (ANN).

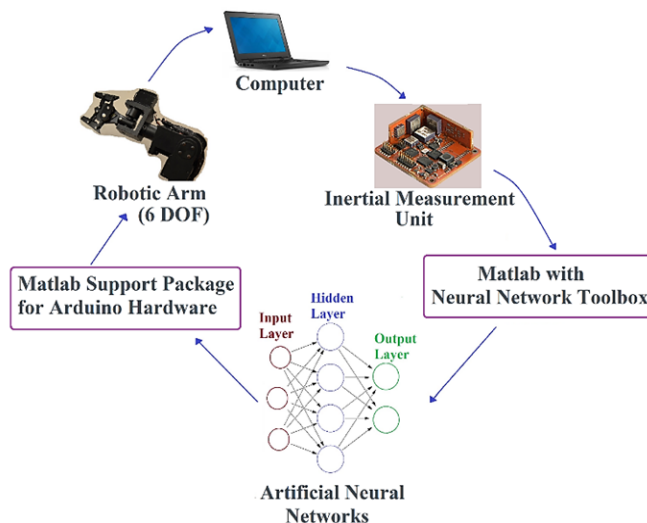


But wireless 6DOF motion tracking is certainly not in its infancy; individuals and companies alike have been working on the technology for decades. And a quick Internet search will yield any number of motion-tracking devices for both persons, objects, and combinations thereof. There are even ads for the esoteric tracking of the movement of chickens—obviously that’s important to some people!

**Subject on the CAREN System
Computer Assisted Rehabilitation Environment (CAREN)**

But for the rest of us, the technology is applicable to the trades (welding, for example), sports (golf, ice skating, weight lifting), hand movements, 3D laser scanning (reverse engineering, archaeological digs, woodworking, rapid prototyping), paint sprayers (well, if we’re going to track chickens, why not paint sprayers?), and of course medical rehabilitation. And WiTrack, using radio reflections, can track not only your body but individual body parts through walls, making it ideal for gaming, monitoring and fall-detection of the elderly, and controlling household appliances.

To get a feel for how the process works, look at the image shown below of the main components of a wireless robotic control system that shows the circular pathway of information flow. In this current study, the robotic arm’s controller had to be trained to distinguish among the arm’s various movements. To make this possible, an ANN was used as a classifier to identify the specific arm movement to perform. The ANN was trained using the backpropagation algorithm and the triaxle acceleration sampling data obtained from the inertial measurement units (IMUs). In the test with an independent subject, the ANN was able to correctly identify eight of the nine motions (88.8%). This accuracy can be improved by expanding the database that was used to train, validate, and test the ANN.



Main Components of the Wireless Robotic Control System

Here are a couple of links to related articles previously published in IJERI and its sister journal IJME (the International Journal of Modern Engineering): *Biomimetic Transfemoral Knee with a Gear Mesh Locking Mechanism* [Ramakrishnan et al. University of South Florida. IJERI fall/winter 2016 v8 n2 pp.30-38] and *The HOAD Research Group Development Process: Hand Opening Assistive Devices for Stroke Victims and the Neurologically Impaired* [Land et al. Johns Hopkins University. IJME spring/summer 2013 v5 n1 pp.41-52].

Editorial Review Board Members

Mohammed Abdallah	State University of New York (NY)	Gengchen Liu	University of California-Davis (CA)
Nasser Alaraje	Michigan Tech (MI)	Guoxiang Liu	University of North Dakota (ND)
Ammar Al-Farga	University of Jiangnan (CHINA)	Louis Liu	University of New Orleans (LA)
Aly Mousaad Aly	Louisiana State University (LA)	Peng Liu	Washington State University (WA)
Paul Akangah	North Carolina A&T State University (NC)	Mani Manivannan	ARUP Corporation
Lawal Anka	Zamfara AC Development (NIGERIA)	G.H. Massiha	University of Louisiana (LA)
Jahangir Ansari	Virginia State University (VA)	Jim Mayrose	Buffalo State College (NY)
Kevin Berisso	Ohio University (OH)	Thomas McDonald	University of Southern Indiana (IN)
Pankaj Bhambri	Guru Nanak Dev Engineering (INDIA)	David Melton	Eastern Illinois University (IL)
Water Buchanan	Texas A&M University (TX)	Shokoufeh Mirzaei	Cal State Poly Pomona (CA)
John Burningham	Clayton State University (GA)	Bashir Morshed	University of Memphis (TN)
Shaobiao Cai	Penn State University (PA)	Sam Mryyan	Excelsior College (NY)
Vigyam Chandra	Eastern Kentucky University (KY)	Jessica Murphy	Jackson State University (MS)
Isaac Chang	Cal Poly State University SLO (CA)	Wilson Naik	University of Hyderabad (INDIA)
Shu-Hui (Susan) Chang	Iowa State University (IA)	Arun Nambiar	California State University Fresno (CA)
Bin Chen	Purdue University Calumet (IN)	Ramesh Narang	Indiana University-Purdue University (IN)
Wei-Yin Chen	University of Mississippi (MS)	Anand Nayyar	Institute Management and Tech (INDIA)
Rigoberto Chinchilla	Eastern Illinois University (IL)	Aurenice Oliveira	Michigan Tech (MI)
Phil Cochrane	Indiana State University (IN)	Reynaldo Pablo	Indiana University-Purdue University (IN)
Emily Crawford	Southern Wesleyan University (SC)	Basile Panoutsopoulos	Community College of Rhode Island (RI)
Brad Deken	Southeast Missouri State University (MO)	Shahera Patel	Sardar Patel University (INDIA)
Z. T. Deng	Alabama A&M University (AL)	Jose Pena	Purdue University Calumet (IN)
Sagar Deshpande	Ferris State University (MI)	Karl Perusich	Purdue University (IN)
David Domermuth	Appalachian State University (NC)	Thongchai Phairoh	Virginia State University (VA)
Dongliang Duan	University of Wyoming (WY)	Huyu Qu	Honeywell Corporation
Marilyn Dyrud	Oregon Institute of Technology (OR)	John Rajadas	Arizona State University (AZ)
Mehran Elahi	Elizabeth City State University (NC)	Vijaya Ramnath	Sri Sairam Engineering College (CHENNAI)
Ahmed Elsayy	Tennessee Technological University (TN)	Desire Rasolomampionona	Warsaw University of Tech (POLAND)
Rasoul Esfahani	DeVry University (OH)	Mohammad Razani	New York City College of Tech (NY)
Dominick Fazarro	Sam Houston State University (TX)	Sangram Redkar	Arizona State University-Poly (AZ)
Ignatius Fomunung	University of Tennessee Chattanooga (TN)	Michael Reynolds	University of Arkansas Fort Smith (AR)
Ahmed Gawad	Zagazig University EGYPT)	Nina Robson	California State University-Fullerton (CA)
Daba Gedafa	University of North Dakota (ND)	Marla Rogers	Wireless Systems Engineer
Mohsen Hamidi	Utah Valley University (UT)	Dale Rowe	Brigham Young University (UT)
Mamoon Hammad	Abu Dhabi University (UAE)	Karen Ruggles	DeSales University (PA)
Gene Harding	Purdue Polytechnic (IN)	Anca Sala	Baker College (MI)
Youcef Himri	Safety Engineer in Sonelgaz (ALGERIA)	Alex Sergeev	Michigan Technological University (MI)
Xiaobing Hou	Central Connecticut State University (CT)	Hiral Shah	St. Cloud State University (MN)
Shelton Houston	University of Louisiana Lafayette (LA)	Siles Singh	St. Joseph University Tanzania (AFRICA)
Kun Hua	Lawrence Technological University (MI)	Ahmad Sleiti	University of North Carolina Charlotte (NC)
Ying Huang	North Dakota State University (ND)	Jiahui Song	Wentworth Institute of Technology (MA)
Dave Hunter	Western Illinois University (IL)	Yuyang Song	Toyota Corporation
Christian Hyeng	North Carolina A&T University (NC)	Carl Spezia	Southern Illinois University (IL)
Pete Hylton	Indiana University Purdue (IN)	Michelle Surerus	Ohio University (OH)
Ghassan Ibrahim	Bloomsburg University (PA)	Jalal Taheri	Bostan Abad Islamic Azad University (IRAN)
John Irwin	Michigan Tech (MI)	Li Tan	Purdue University Northwest (IN)
Toqeer Israr	Eastern Illinois University (IL)	Harold Terano	Camarines Sur Polytechnic (NABUA)
Sudershan Jetley	Bowling Green State University (OH)	Sanjay Tewari	Louisiana Tech University (LA)
Rex Kanu	Ball State University (IN)	Vassilios Tzouanas	University of Houston Downtown (TX)
Tolga Kaya	Central Michigan University (MI)	Jeff Ulmer	University of Central Missouri (MO)
Satish Ketkar	Wayne State University (MI)	Mihaela Vorvoreanu	Purdue University (IN)
Manish Kewalramani	Abu Dhabi University (UAE)	Phillip Waldrop	Georgia Southern University (GA)
Tae-Hoon Kim	Purdue University Calumet (IN)	Abraham Walton	Purdue University (IN)
Chris Kluse	Bowling Green State University (OH)	Haoyu Wang	Central Connecticut State University (CT)
Doug Koch	Southeast Missouri State University (MO)	Liangmo Wang	Nanjing University of Science/Tech (CHINA)
Ognjen Kuljaca	Brodarski Institute (CROATIA)	Boonsap Witchayangkoon	Thammasat University (THAILAND)
Chakresh Kumar	Uttar Pradesh Tech University (INDIA)	Alex Wong	Digilent Inc.
Zaki Kuruppallil	Ohio University (OH)	Shuju Wu	Central Connecticut State University (CT)
Edward Land	Johns Hopkins Medical Institute	Baijian "Justin" Yang	Ball State University (IN)
Jane LeClair	Excelsior College (NY)	Eunice Yang	University of Pittsburgh Johnstown (PA)
Shiyong Lee	Penn State University Berks (PA)	Mijia Yang	North Dakota State University (ND)
Soo-Yen Lee	Central Michigan University (MI)	Xiaoli (Lucy) Yang	Purdue University Calumet (IN)
Solomon Leung	Idaho State University (ID)	Faruk Yildiz	Sam Houston State University (TX)
Chao Li	Florida A&M University (FL)	Yuqiu You	Morehead State University (KY)
Jimmy Linn	Eastern Carolina University (NC)	Pao-Chiang Yuan	Jackson State University (MS)
Dale Litwhiler	Penn State University (PA)	Jinwen Zhu	Missouri Western State University (MO)

THE IMPLEMENTATION OF RECYCLED THERMOSETTING COMPOSITE POWDER IN ROTATIONAL CASTING

Dru M. Wilson, Central Michigan University

Abstract

Is it possible to grind up used or damaged composite products into powder and use it as filler in rotational casting? Rotational casting is a good candidate for this research method, since the percentage of recycled powder can be confirmed and maintained during this process. The exact amount of virgin plastic and recycled powder is placed directly into the mold and then closed, allowing all of the material to stay in the mold. The approach in this current study was not to return the fiberglass with polyester resin back to pre-mixed conditions, but to grind a used composite product into powder and use it as a filler. This concept could have a positive impact in two areas: it could reduce the amount of composite products in landfills or junkyards, and it can reduce the amount of virgin material needed to produce each new part. The samples with filler were evaluated using three methods: observational, drop test, and compression test.

Introduction

Rotational casting, also known as rotational molding or rotomolding, is a plastics manufacturing process that uses thermoplastic powder to produce hollow products. The powder is placed into a hollow mold and rotated on both major and minor axes. This allows the plastic to tumble inside the mold cavity allowing it to adhere to the mold as it is heated [1, 2]. To produce fiberglass composite products, fiberglass reinforcement must be saturated with resin to make the final part structurally rigid. Two of the primary functions of the resin are to transfer stress to the individual strands of fiberglass and to hold the fibers in the proper orientation (including geometrical shape). The most common types of resin are polyester, epoxy, vinyl ester, and urethane; all four are thermosetting (or thermosets) resins. Once a thermosetting resin has chemically cross-linked, or cured, it is virtually impossible to reverse or recycle. Once a composite product has cured, it will not chemically “reset” back to a premixed liquid resin.

As a result, there are composite products in landfills across the country that will never decompose. Examples include boats, showers, bathtubs, car bumpers, aircraft parts, campers, and canoes. This is a growing problem and will continue to increase until alternative solutions can be found

in reusing the disposed composites. According to Thomas et al. [3], “Recycling of thermosetting polymers is regarded as one of the urgent problems to be settled because of its technological difficulty.” Currently, fiberglass/resin composite recycling can be divided into mechanical, conventional pyrolysis, microwave pyrolysis, and chemical and electrical fragmentation-based processes [3, 4]. However, these methods can be time consuming and extremely costly. According to Lopez et al. [5], “The recycling of these composites is not, at present, profitable in economic terms, because obtained fibers present lower mechanical properties than the original ones, and cannot be employed in the manufacture of structural materials. Therefore, most of the waste glass fiber composites are stored in landfills or buried. This causes serious environmental problems, due to this kind of wastes are usually non-biodegradable and very bulky.”

Rotational casting products can be classified into many areas, including toys, agricultural products, automotive products, boats, kayaks, road safety, industrial products, lighting, and furniture [1, 6]. Various shapes and sizes of kayaks are great examples of rotational casting. Polyethylene (PE) is the industry standard plastic for producing kayaks. Using recycled thermoplastics (including PE) in the rotational casting process has been successfully practiced since the 1980s [7]. Thermoplastics are significantly different from thermosetting plastics, because they can be easily re-melted and re-used. Unfortunately, thermosetting plastics are not commonly used in rotational molding. However, if a small percentage of recycled fiberglass/polyester powder could be used in the manufacturing process, it would reduce that amount of virgin PE material needed.

Table 1 gives a breakdown of how a company can reduce virgin PE. For example, if a company can make 500 kayaks a day, and each weighs 30 pounds, 1500 pounds of PE will be needed per day. Is it possible to remove a damaged one-piece fiberglass/polyester bathtub/shower unit, weighing approximately 120 pounds, from a landfill and grind it up into a powder? This recycled powder could then be used, in small percentages, in producing kayaks. There would be two major benefits. It would reduce the amount of virgin PE material, while eliminating a large damaged fiberglass product out of landfill. If 10 percent filler were possible, it would reduce the PE amount by 150 pounds per day. This appears to be minimal, but would save 4000 pounds in a

year. The more significant benefit would be the elimination of 1.25 damaged fiberglass bathtub/showers each day, or over 450 bathtub/showers a year.

Table 1. Weight Analysis Using the Kayak Example: Manufacturing 500 Kayaks per Day Using 30 Pounds of High-Density Polyethylene (HDPE) per Kayak Recycled Fiberglass/Polyester (F/P) Powder Filler

% of F/P Powder	HDPE Usage (lb)		F/P Powder (lb)		Bathtub Reduction	
	Daily	Yearly	Daily	Yearly	Daily	Yearly
0%	1500.0	547,500	n/a	n/a	n/a	n/a
2.5%	1462.5	533,813	37.5	13,688	0.31	114.06
5%	1425.0	520,125	75.0	27,375	0.63	228.13
7.5%	1387.5	506,438	112.5	41,063	0.94	342.19
10%	1350.0	492,750	150.0	54,750	1.25	456.25

A cost analysis using virgin HDPE and recycled fiberglass/polyester powder as a filler was completed. The average price for HDPE powder is approximately \$0.60 per pound, when buying a minimum of 2205 pounds [8]. The cost of the fiberglass/polyester powder was more difficult to calculate. After looking at various parameters (labor, time, equipment, etc.) a cost of \$0.38 per pound was determined as shown in Table 2.

Table 2. Cost of Recycled Fiberglass/Polyester Powder

Item	Cost	Notes
Labor	\$20 per hour	Manual labor for one operator
Equipment	\$150 per hour	Includes equipment, maintenance, facilities, utilities, etc.
Collection Fee	(\$20 per hour)	Companies can charge \$100 to collect 2000 pounds of damaged fiberglass. Cost per pound (\$0.05) multiplied by one hour of work (400 pounds) equals \$20 per hour
Production Cost	\$150 per hour	Labor + Equipment – Collection Fee
F/P Powder Production	400 pounds per hour	Takes ½ hour to grind 400 pounds; must grind material twice to reduce fiberglass rods into powder
Final Cost	\$0.38 per pound	\$150 ÷ 400 pounds = \$0.375 rounding up to \$0.38

Spent fiberglass products are readily available and can be obtained free. In fact, there are recycling companies that are charging a collection fee to haul away damaged fiberglass boats. These prices range from \$325 to \$2400 depending on the size of the fiberglass boat [9]. Eco-Wolf, Inc. sells equipment that can grind over 800 pounds of cured fiberglass an hour. The amount of fiberglass that can be chopped per hour is impressive; unfortunately, substituting the chopped fiberglass powder (rod length of 3175-25400 µm, or 0.3175-2.54 cm) for the recycled fiberglass/polyester powder (rod length of 50-150 µm) would not be acceptable [9]. This discrepancy in rod length could be resolved by running the chopped fiberglass rods through the grinding equipment twice and then using a strainer to remove any remaining larger rods from the new powder.

Table 3 shows how a company can save \$12,045 per year by implementing 10% recycled fiberglass/polyester powder into their products. Not only can a company achieve an annual savings of 3.67%, they will also have a positive impact on the environment by reducing the amount of virgin materials used (i.e., natural resources), while eliminating damaged composite products from the landfills.

Table 3. Cost Analysis Using the Kayak Example from Table 1: Based on High-Density Polyethylene (HDPE) at \$0.60/pound and Recycled Fiberglass/Polyester (F/P) Powder at \$0.38/pound

% of F/P Powder	Daily Cost		Total Cost (HDPE + F/P powder)		Total Savings (\$)
	HDPE	F/P powder	Daily	Yearly	Yearly
0%	\$900.00	n/a	\$900.00	\$328,500.00	n/a
2.5%	\$877.50	\$14.25	\$891.75	\$325,488.75	\$3011.25
5%	\$855.00	\$28.50	\$883.50	\$322,477.50	\$6022.50
7.5%	\$832.50	\$42.75	\$875.25	\$319,466.25	\$9033.75
10%	\$810.00	\$57.00	\$867.00	\$316,455.00	\$12045.00

Material and Sample Preparation

The powder was produced by using a die grinder to grind up composite panels consisting of fiberglass with polyester resin. Once the powder was collected, it was sifted through a food strainer twice to reduce the particle size to the approximate size of the virgin high-density polyethylene (HDPE) powder commonly used in rotational casting. The recycled fiberglass/polyester powder was analyzed under a

scanning electronic microscope (SEM). Figures 1-3 clearly show that, during the grinding process, the polyester resin separated cleanly from the fiberglass rods. The polyester resin became like small granular rocks, with the majority being between 10-150 μm . The fiberglass rods broke relatively smoothly, with the majority of the rods being 7-10 μm in diameter and 50-150 μm in length.

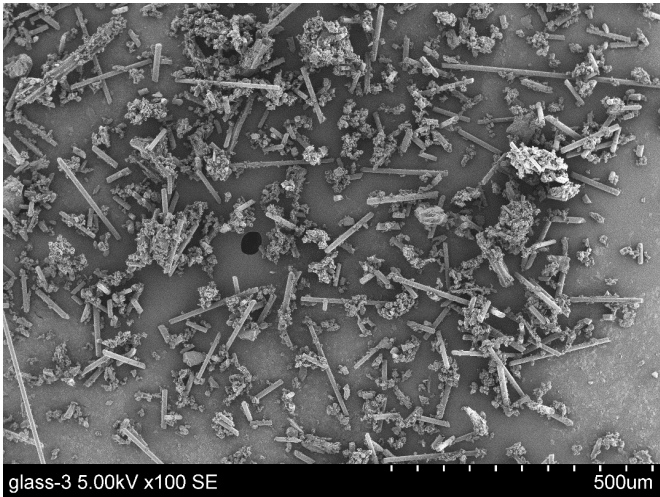


Figure 1. Scanning Electron Microscope (SEM) Image of Recycled Fiberglass/Polyester Powder (500 μm)

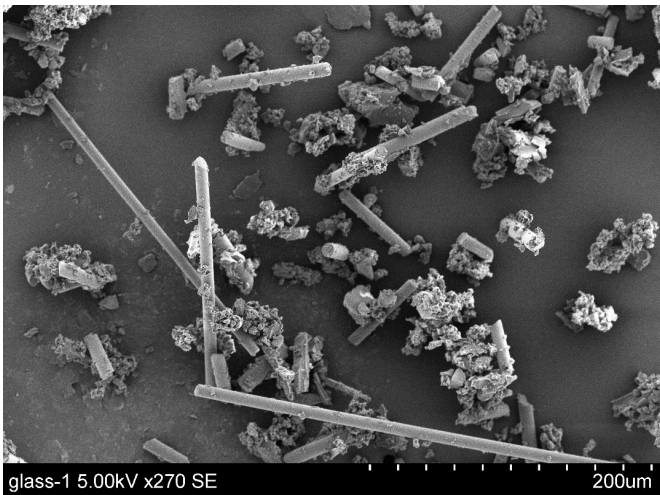


Figure 2. Scanning Electron Microscope (SEM) Image of Recycled Fiberglass/Polyester Powder (200 μm)

After producing a few trial samples (8.5 cm hollow balls), the authors decided to use recycled fiberglass/polyester powder at 2.5% increments up to 10% filler. The trial sample piece at 12.5% filler was getting “clumpy” and the recycled powder wanted to cling to itself, making noticeable imperfections in the final product. By using increments of 2.5%, there were slightly noticeable differences in texture and color; smaller percentage increments did not appear to

produce any differences. A control group (samples with zero percent recycled powder) was created to have a standard for comparison to the parts with the various percentages of recycled powder. Table 4 gives a breakdown of the amount of HDPE and fiberglass/powder used for each sample piece.

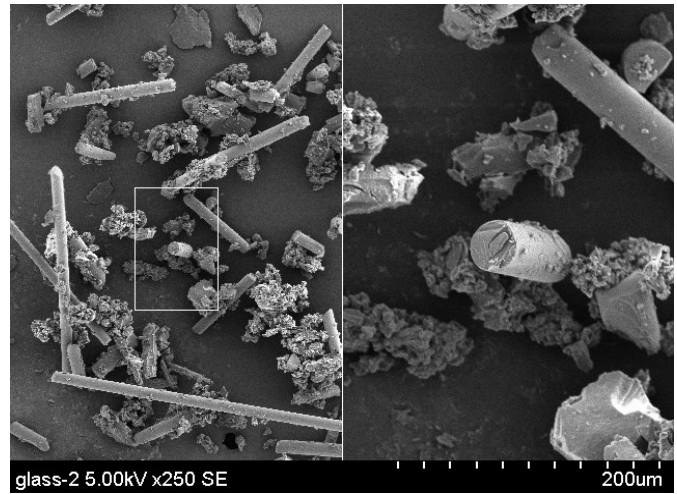


Figure 3. Scanning Electron Microscope (SEM) Image of Recycled Fiberglass/Polyester Powder (image on the right is a high-magnification shot of the area inside the rectangle)

The fiberglass/polyester (F/P) powder was weighed using a digital scale capable of measuring to 0.0000g. For each rotational casting product, the virgin material and recycled powder ratios were weighed individually to maintain accuracy. The recycled powder was then added to the virgin material and stirred for two minutes before being poured into the rotational mold. To maintain control standards, the same procedures were used for making all 25 sample pieces. The premixed F/P powder was poured into a 350°F preheated mold. The temperature was then increased to 400°F while the mold was being rotated around the major axis at 15 rpm for 30 minutes. The mold rotated for another 30 minutes with the heat turned off and the oven door opened, allowing the plastic ball to cool. After cooling, the sample was removed from the mold and labeled.

Testing and Results

Observational

Besides collecting data, a visual inspection was done on each test piece. Each ball was visually inspected for color and surface texture. With the increase in recycled fiberglass/polyester filler, there were obvious changes in color and surface porosity. The color of the sample pieces become noticeably darker. The samples that had zero percent filler

were an opaque white color, but with each additional increase in filler percentage, the samples became noticeably darker or “dirtier.” Figure 4 shows how the sample colors went from white, off-white, beige, tan, and dark tan, respectively.

Table 4. High-Density Polyethylene (HDPE) and Fiberglass/ Polyester (F/P) Powder Material Usage

Sample Piece #	Filler Percentage	HDPE	F/P Powder
1	0%	60.00 g	--
2	0%	60.003 g	--
3	0%	60.004 g	--
4	0%	60.003 g	--
5	0%	60.002 g	--
6	2.5%	58.501 g	1.504 g
7	2.5%	58.501 g	1.502 g
8	2.5%	58.502 g	1.502 g
9	2.5%	58.502 g	1.503 g
10	2.5%	58.502 g	1.502 g
11	5%	57.002 g	3.002 g
12	5%	57.002 g	3.002 g
13	5%	57.001 g	3.003 g
14	5%	57.002 g	3.001 g
15	5%	57.002 g	3.001 g
16	7.5%	55.502 g	4.501 g
17	7.5%	55.501 g	4.502 g
18	7.5%	55.502 g	4.501 g
19	7.5%	55.502 g	4.502 g
20	7.5%	55.502 g	4.502 g
21	10%	54.002 g	6.002 g
22	10%	54.002 g	6.002 g
23	10%	54.002 g	6.001 g
24	10%	54.001 g	6.001 g
25	10%	54.002 g	6.002 g



Figure 4. Samples Produced with 0%, 2.5%, 5%, 7.5%, and 10% Fiberglass/Polyester Powder (left to right)

Figures 5-7 show that the surface porosity for the samples with 0%, 2.5%, and 5% filler looked virtually the same. This demonstrates that small percentages of fiberglass/ polyester powder, when distributed evenly in the samples, would fuse with the HDPE.



Figure 5. Samples with 0% Filler



Figure 6. Samples with 2.5% Filler



Figure 7. Samples with 5% Filler

Figure 8 shows that, for the samples with 7.5% filler, there were small pinhole voids on the entire surface of the ball, along with one or two small pockets of clumped fiberglass. The voids were in the top skin-surface only, and did not go completely through the part.



Figure 8. Samples with 7.5% Filler and Having Small Pinhole Voids over Their Entire Surface

Figure 9 shows that balls with 10% filler had two obvious quality issues. There were small pinhole voids over the entire surface, just like the samples with 7.5% filler. The second issue was the amount of noticeable small pockets of clumped fiberglass over the entire surface of the ball. If a company wanted to have a greater impact on the environment, this could still be an option if the products were painted or used in an unseen location.

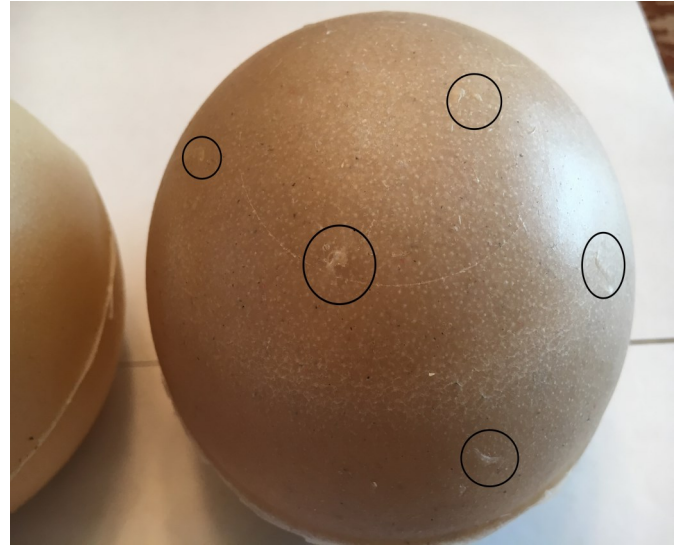


Figure 9. Samples with 10% Filler and Having Small Pinhole Voids and Numerous Pockets of Clumped Fiberglass/Polyester Powder (located inside the circles) over Their Entire Surface

Drop Test

The second test performed was a two-meter drop test. Each ball was placed in a container with a sliding bottom. The bottom of the container was quickly pulled, causing the ball to drop down and bounce off the concrete floor. A large cardboard ruler with horizontal lines was used as the backdrop to determine the bounce height. Table 5 shows the data collected for the drop test, which was completed in one setting. During a trial run to determine drop height, it was determined that two meters produced the best consistency of the ball bouncing. At one meter, the balls had minimal bounce; at three meters, the balls would bounce at inconsistent and random angles. Each sample piece (ball) was dropped from the same height without a guide system. Using a tube or pole for a guide would have caused the ball to skip off the tube, causing a reduction in true speed.

Table 5 shows that all five balls from the control group (0% filler) bounced over 100 cm. For all of the test pieces with filler, only three balls (out of 20) bounced over 100 cm, and none of the filler percentages had more than one ball that bounced over 100 cm. The control group had the best standard deviation (1.483) followed by 2.5% filler (3.912). The standard deviation for 5% filler would have been the lowest if not for one ball, since the other four balls with 5% filler bounced to $88\text{cm} \pm 1\text{cm}$. The balls using 5%, 7.5%, and 10% filler, were very similar in bounce average and also had the highest three standard deviations. Based solely on the drop test data, the best sample of balls were the control group (0% filler); however, balls with 2.5% filler

presented a viable option. The balls with 2.5% filler only had an 8.615% reduction in bounce at three meters and had the second best standard deviation. Figure 10 shows the averages of the bounce height for each sample set, which tended to decrease when higher percentages of filler were used.

Table 5. Drop Test (Bounce) Results

Test Piece #	Filler Percentage	Bounce Height	Average (Std. Dev.)
1	0%	107 cm	
2	0%	107 cm	
3	0%	105 cm	
4	0%	109 cm	106.8 cm (1.483)
5	0%	106 cm	
6	2.5%	98 cm	
7	2.5%	92 cm	
8	2.5%	103 cm	
9	2.5%	97 cm	97.6 cm (3.912)
10	2.5%	98 cm	
11	5%	89 cm	
12	5%	87 cm	
13	5%	104 cm	
14	5%	88 cm	91.2 cm (7.190)
15	5%	88 cm	
16	7.5%	84 cm	
17	7.5%	101 cm	
18	7.5%	87 cm	
19	7.5%	90 cm	89.4 cm (6.877)
20	7.5%	85 cm	
21	10%	87 cm	
22	10%	91 cm	
23	10%	90 cm	
24	10%	93 cm	91.8 cm (4.087)
25	10%	98 cm	

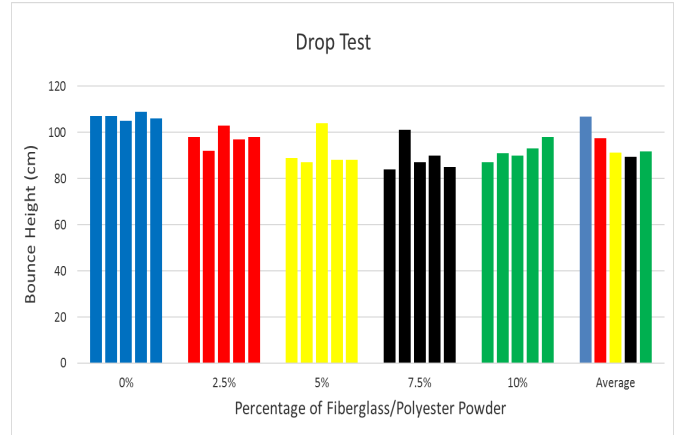


Figure 10. Drop-Test Results Using Various Ratios of Recycled Fiberglass/Polyester Powder

Compression Test

The third, and final test, was the compression test. An Instron Model 5582 with a load cell of 100 kN was used to test the balls. Each ball was placed on the bottom fixture mount, while a flat steel plate attached to the top fixture was used to apply the compression load. The compression load was applied at 2.5 cm per minute. Table 6 shows the data collected for the compression test, which was completed in one setting.

The 2.5% filler group had the best compression load average (4.208 kN), followed by the 0% group (4.098 kN). Balls with 0% and 2.5% filler had four out of five results above 4.0 kN. The 2.5% filler group had three out of the four highest compression results of all the balls. The group with 7.5% filler had the most inconsistent results, with three results above 4.0 kN, and also had the lowest two compression results for all percentage groups. Averages of the compression load tests for each sample set tended to decrease when higher percentages of filler were used.

All five sample groups had low standard deviations, ranging from 0.107 (0% filler) to 0.525 (7.5% filler). Table 6 shows that the balls with 2.5%, 5%, and 10% had similar standard deviation results of 0.234, 0.235, and 0.289, respectively. Based solely on the compression test, the balls with 2.5% filler performed the best. The 2.5% samples had the highest compression load average (4.208 kN) along with a relatively low standard deviation (0.289). The second choice would be the control group (0% filler), based on the second highest compression result (4.098 kN) and the lowest standard deviation (0.107). Figure 11 shows that the samples with 0% and 2.5% filler had higher compression maximum load results, while fillers with 5%, 7.5% and 10% tended to have lower results.

Table 6. Compression Test Maximum Load Results

Test Piece #	Filler Percentage	Maximum Load	Average (Std. Dev.)
1	0%	4.12 kN	
2	0%	4.19 kN	
3	0%	4.03 kN	
4	0%	3.95 kN	4.098 kN (0.107)
5	0%	4.20 kN	
6	2.5%	4.31 kN	
7	2.5%	3.72 kN	
8	2.5%	4.42 kN	
9	2.5%	4.18 kN	4.208 kN (0.289)
10	2.5%	4.41 kN	
11	5%	4.37 kN	
12	5%	3.85 kN	
13	5%	3.83 kN	
14	5%	3.82 kN	3.952 kN (0.235)
15	5%	3.89 kN	
16	7.5%	3.16 kN	
17	7.5%	4.09 kN	
18	7.5%	4.01 kN	
19	7.5%	4.28 kN	3.750 kN (0.525)
20	7.5%	3.21 kN	
21	10%	3.82 kN	
22	10%	3.46 kN	
23	10%	4.04 kN	
24	10%	3.62 kN	3.774 kN (0.234)
25	10%	3.93 kN	

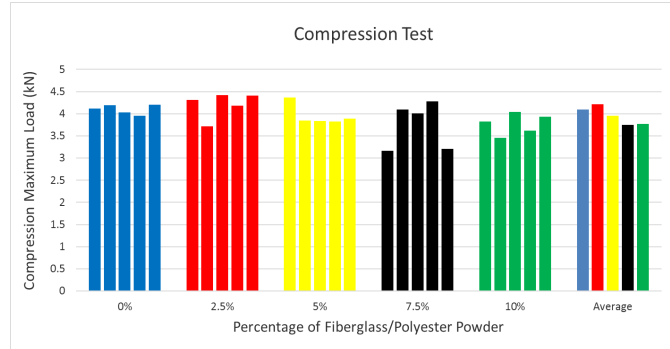


Figure 11. Compression-Test Results Using Various Ratios of Recycled Fiberglass/Polyester Powder

Conclusions

A study was conducted in order to determine if recycled fiberglass/polyester (F/P) powder could be implemented in rotational casting. Various filler percentages (0%, 2.5%, 5%, 7.5%, and 10%) were added to virgin high-density polyethylene (HDPE) powder to produce round, hollow balls. The balls were then evaluated by general observation, drop testing, and compression testing. After manufacturing, testing, and analyzing the results, the control group (0% filler) performed the best overall. It had the best color, highest drop test bounce results (106.8 cm), and was second in the compression test. The balls with 2.5% filler also performed well, with color being slightly darker; they were second in the drop test (97.6 cm) and best in the compression test (4.208 kN). A company willing to have less than a 10% reduction in bounce could advertise a ball with recycled fiberglass/polyester filler as an environmentally friendly or “green” product.

According to Tables 1 and 3, using the kayak and bathtub examples, even a small substitution using only 2.5% filler could help reduce the size of landfills by 114 bathtubs and save \$3011.25 in virgin HDPE per year. Based on the overall results, the three higher filler percentages (5%, 7.5%, and 10%) were similar to each other. These sample pieces were darker, had less bounce, and had lower compression strengths. The higher filler percentages did not have ideal results, but could still be considered a viable option, depending on the use and geometric shape of the product, or if the customer wants an environmentally friendly product.

Acknowledgements

The scanning electron microscope (SEM) slides used in Figures 1-3 were produced by Philip E. Oshel. Mr. Oshel is the Microscopy Facility Supervisor, located in the Department of Biology at Central Michigan University.

References

- [1] Lokensgard, E. (2016). *Industrial Plastics: Theory and Applications*. (6th ed.). Cengage Learning.
- [2] Strong, A. (2006). *Plastics: Materials and Processes*. (3rd ed.). Pearson.
- [3] Thomas, R., Vijayan, P., & Thomas, S. (2011). Recycling of thermosetting polymers: Their blends and composites. In A. Fainleib & O. Grigoryeva (Eds.), *Recent Developments in Polymer Recycling* (pp. 121-153). India: Transworld Research Network.
- [4] Shuaib, N. A., & Mativenga P. T. (2016). Energy Demand in Mechanical Recycling of Glass Fibre Reinforced Thermoset Plastic Composites. *Journal of Cleaner Production*, 120, 198-206.
- [5] Lopez, F., Martin, M., Garcia-Diaz, I., Rodriguez, O., Alguacil, F., & Romero, M. (2012). Recycling of Glass Fibers from Fiberglass Polyester Waste Composite for the Manufacture of Glass-Ceramic Materials. *Journal of Environmental Protection*, 3, 740-747.
- [6] Crawford, R. J., & Kearns, M. P. (2012). *Practical Guide to Rotational Moulding*. (2nd ed.). Smithers Rapra Technology.
- [7] Voldner, E. (2016). Recycling & Rotational Molding. *RotoWorld*. Retrieved from <https://rotoworldmag.com/recycling-rotational-molding>.
- [8] Alibab.com Global Trade Starts Here. (n.d.) Retrieved from <https://www.alibaba.com/showroom/hdpe-powder.htm>.
- [9] Flannery, J. (2017). The dead-boat disposal crunch. *Soundings Trade Only Today*. Retrieved from <https://www.tradeonlytoday.com/features/dealers/marinas-boatyards/the-dead-boat-disposal-crunch>.

Biographies

DRU M. WILSON is an associate professor in the School of Engineering and Technology at Central Michigan University. He earned his BS and MS degrees from Purdue University, and PhD from Iowa State University. His interests include plastics and composite manufacturing, recycling alternatives, prototyping, and engineering technology education. Dr. Wilson may be reached at wilson1dm@cmich.edu

WIRELESS CONTROL OF A ROBOTIC ARM USING 3D MOTION TRACKING SENSORS AND ARTIFICIAL NEURAL NETWORKS

Fernando Ríos, Georgia Southern University; Rocío Alba-Flores, Georgia Southern University; Imani Augusma, Georgia Southern University

Abstract

In this paper, the authors describe the hardware and software components of an intelligent system that is able to wirelessly control the movements of a robotic arm for mimicking human arm gestures. For the implementation of the system, a laptop computer, 3D wireless motion tracking sensors, an artificial neural network (ANN) classifier, and a microcontroller were used to drive the six-degree-of-freedom robotic arm. Results demonstrated that the robotic arm is capable of mimicking motions of the human arm. The overall accuracy of the ANN classification system was 88.8%. Due to limitations of non-continuous rotation servos, some movements had to be limited or changed in order for the robotic arm to perform as an equivalent to a human arm.

Introduction

Robotic technologies have played and will continue to play important roles in helping to solve real-life problems. One of the most important fields in the development of successful robotic systems is the human-machine interaction (HMI). In this paper, the authors describe the development of a system that uses an ANN classifier to control a robotic arm that is able to mimic the movements of a human arm. In this study, the user was able to directly control a six-degree-of-freedom (6-DOF) robotic arm by performing arm motions with his/her own arm. The system uses inertial measurement units to sense the movements of the human arm.

Alternative approaches that have been used to develop human-machine interaction include the use of electromyography (EMG) signals to capture and analyze electrical activity in human muscle tissue [1, 2]. However, due to the electrical signals being minuscule, processing the data using this method is difficult. Other techniques that have been used include gyroscopes and accelerometers. For example, Sekhar et al. [3] developed a low-cost wireless motion sensing control unit using three sensors: accelerometer, gyroscope, and magnetometer. They used a three-degree-of-freedom robotic arm to control the elbow and wrist positions. Matlab software was used to process the signals coming from the

sensors and generate the pulse width modulation (PWM) signals to control the servomotors; the accuracy of the developed system was not specified. An alternate approach that recently has started to gain popularity among researchers is to track muscle activity using inertial measurement units (IMUs) and air pressure sensors [4, 5]. IMUs integrate an accelerometer, a gyroscope, and a magnetometer together to measure three-directional static and dynamic movements. Malegam and D'Silva [6] developed a mimicking robotic hand-arm using flex sensors for individual fingers and multiple three-axis accelerometers. Using four encoders, they divided individual processing units for the fingers and arm to increase the processing speed. They also used a high-speed microcontroller to control the input and output processing, then developed a glove to house all of the components for a user to wear.

Tracking System Operation

In this current study, the authors designed and developed a wireless control system to give commands to a robotic arm. The commands were given by a human subject wearing two IMUs on his/her arm. Figure 1 shows the selected IMU location. The IMU contained an accelerometer, a gyroscope and a filter in a small unit [7]. The robotic arm had six degrees of freedom and could perform elbow, wrist, and shoulder joint movements. Figure 2 shows the robotic arm used in this study. Kalman filtering was also integrated into the IMU software to reduce potential noise and to produce smooth signal data.



Figure 1. Subject Wearing the Two Inertial Measurement Units (IMUs)

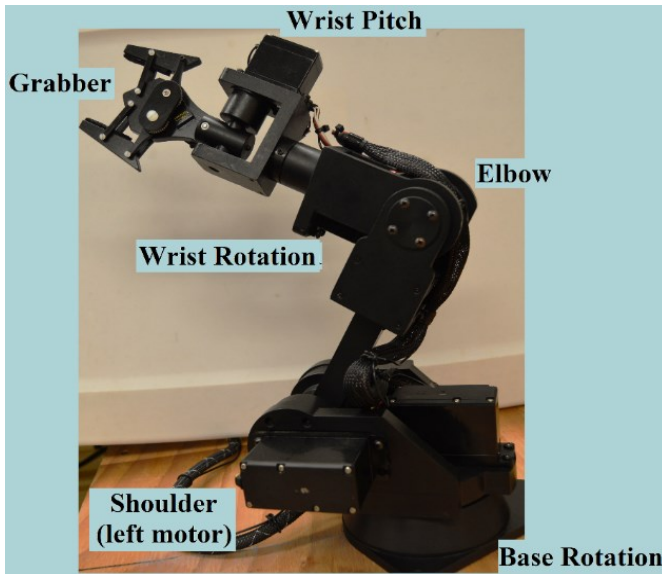


Figure 2. Six-DOF Robotic Manipulator

After obtaining movement activity information from the IMUs, the data were then fed into a trained ANN. An ANN is an adaptive and powerful artificial intelligence (AI) technique that is used to classify the inputs of a biological system. The ANN has the ability to recognize both linear and nonlinear relationships between input and output data, similar to the human brain. Because of this, ANNs are widely used for data classification and pattern recognition. Figure 3 shows the basic structure of an ANN.

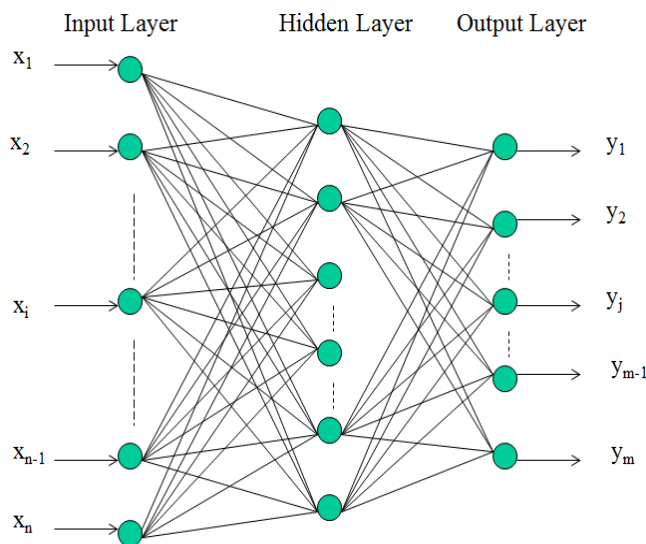


Figure 3. Schematic Diagram of a Multilayer Feed-Forward Neural Network

The ANN processes information using various layers that are linked together: the input layer, the hidden layer, and the

output layer. Each layer is composed of interconnected nodes that represent neurons. Data are fed into the input layer, which connects to the hidden layer, and the hidden layer connects that output to the output layer. All of the connections are weighted, and individual weights are modified as the network is trained. The ANN learns by example, using an algorithm called backpropagation, also known as the backwards propagation error. The ANN receives input data repeatedly and then makes a guess about the corresponding output and then compares it to the actual output. The hidden layer computes an error that will be fed back into the network to adjust the weights. Each input and hidden layer neuron's value is multiplied by a predetermined weight. The weights are meant to minimize the error as much as possible to minimize misclassifications.

The weighted input layer and the weighted hidden layer are then summed together. If the summation does not equal one, then adjustments will occur during each cycle, or "epoch," until the summation is as close to one as possible, which means the error cannot be minimized further and this input corresponds to an output. This is called training the ANN. Rote memorization can occur if the network is trained to recognize only one type of input. This is called over-training the system. For an ANN to work properly, it must be trained with various types of input data to a desired output. After training the system, it will be able to see new input data and adjust the weights accordingly in order to produce an accurate output [8-11]. The ANN then determines the corresponding movement that is performed by the user, based on the test set that was used to train the ANN. After the network decides the movement, this information is sent to the robotic arm to emulate the human arm motion.

Main System Components

Figure 1 shows the 3D wireless motion tracking sensors IMUs [7] that were placed on the human subject's arm at two locations—the wrist and the upper arm. At a sampling rate of 100 Hz, the sensors tracked the XYZ-coordinates, inertial data, and the Euler angles of the subject's arm as he/she performed a specific movement. Nine pre-defined arm motions were selected for detection in this study. The raw data (XYZ-coordinates from the IMUs) were processed computing the root mean square (RMS) and the average rectified value (ARV). Normalized data were then used to train a multilayer, feed-forward ANN to classify the arm motions. The Matlab Neural Network toolbox software was used for the design and implementation of the ANN classifier. An Arduino microcontroller was used to control the servo motors in the robotic arm. The Arduino was directly interfaced to the laptop computer implementing the ANN classifier. The data set used for training the ANN in this

study consisted of 180 data vectors (from four different subjects, each of which performed each motion five times). Seventy percent of the data was used for training the ANN, 10% for validation, and 20% for testing. A totally independent set of arm motions (from a 5th subject) was used to determine the accuracy of the ANN classification system.

The main components used in the implementation of the system were: a) an IMU board composed of a digital three-axis accelerometer and a digital three-axis gyroscope [7]; b) a ZigBee RF wireless communication module [12] to transmit and receive data; c) a low-cost microcontroller, Arduino Mega [13], to control the input and output processing; d) a 6-DOF robotic arm that used servo motors to control the joint positions (see again Figure 2)—the servos were controlled using PWM signals; and, e) a Kalman filter that was used to reduce noise and have smooth signal data from the accelerometers and the gyroscope. Figure 4 shows the interaction of these components.

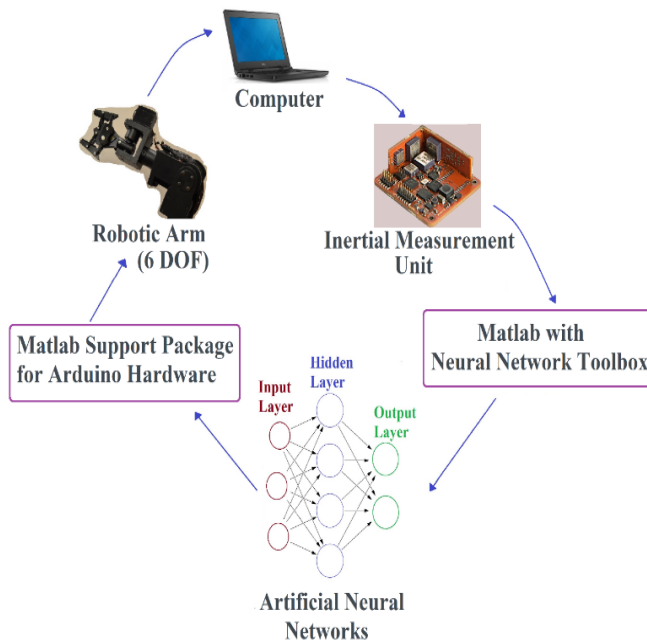


Figure 4. Main Components of the Wireless Robotic Control System

Methods

The human subject performed one of the pre-defined arm movements and Xsens Technologies' [7] software captured the waveform of the acceleration data. These data were then exported into an Excel spreadsheet and imported into Matlab. The sampling rate of the sensors was 100 Hz and each arm movement took approximately three seconds to perform. After the sensor data were collected, Matlab func-

tions were used to calculate the RMS and ARV values. These values are then fed into the trained ANN. The ANN then determined the corresponding arm movement that was performed by the human subject. The corresponding arm movement was then performed by the robotic arm.

Description of the Arm Movement

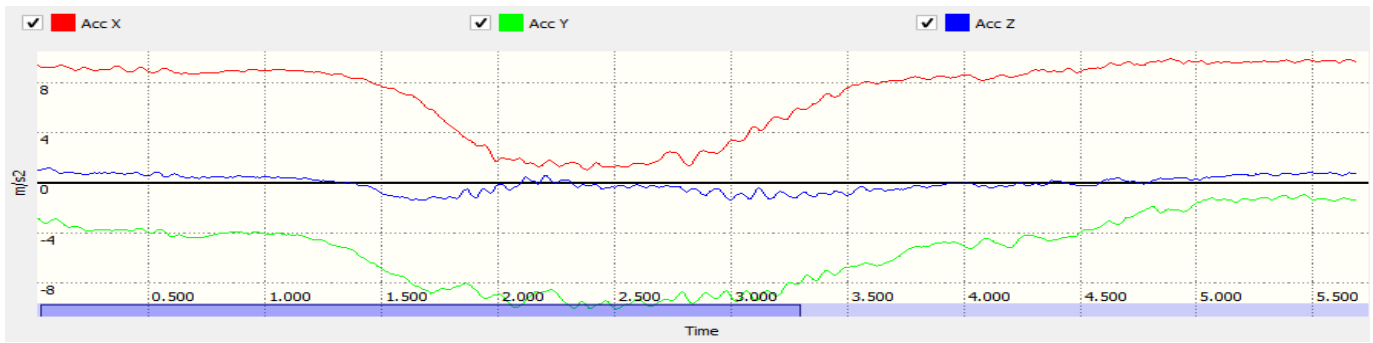
To capture the arm's movements, two IMUs were used. Figure 2 shows that sensor 1 was placed on the person's upper arm and sensor 2 was placed closest to the wrist. Sensor 1 signifies the unit on the person's upper arm and sensor 2 signifies the unit on the person's wrist. There was a total of nine pre-defined arm movements that the ANN could identify and the robotic arm could mimic—arm extension, arm raise, arm raise elbow bend, clockwise windmill, counterclockwise windmill, shoulder touch, side arm raise, wipe right, and wrist rotation. Figure 1 shows that the arm movement used the same initial position—straight down by the person's side, fingers pointing to the floor. For all of the following descriptions of arm movements, the initial starting position was for the person to be standing, the arm and hand fully extended on the side of the body, and the palm facing the body.

Motion 1: Arm Extension. When performing the arm extension movement from the starting position, the person first bends the elbow until the forearm is parallel to the floor, then extends the full arm all the way forward, maintaining it parallel to the floor, and then returns to the initial position. Figure 5 shows the acceleration waveforms obtained during the arm extension motion.

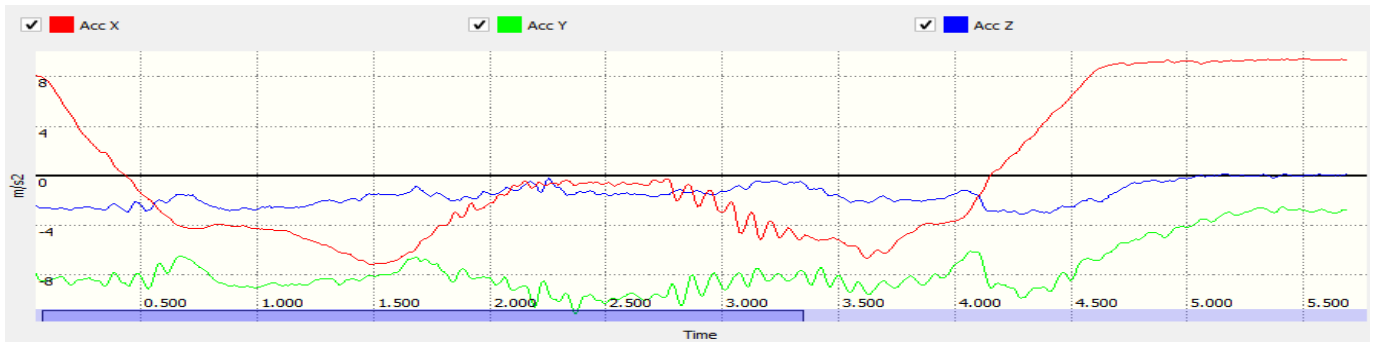
Motion 2: Arm Raise. When performing the arm raise movement, the person starts in the initial position. Without bending the elbow, the person raises the arm up to shoulder height and then returns to the initial position. Figure 6 shows the acceleration waveforms obtained during the arm raise motion.

Motion 3: Arm Raise Elbow Bend. When performing the arm raise elbow bend movement, the person starts from the initial position, next raises the full arm to shoulder height, bends the elbow inwards towards the body until the forearm touches the biceps, and then returns to the initial position. Figure 7 shows the acceleration waveforms obtained during the arm raise elbow bend motion.

Motion 4: Clockwise Windmill. When performing the clockwise windmill from the initial position, the person rotates the shoulder 360 degrees clockwise and then returns to initial position. Figure 8 shows the acceleration waveforms obtained during the clockwise windmill motion.

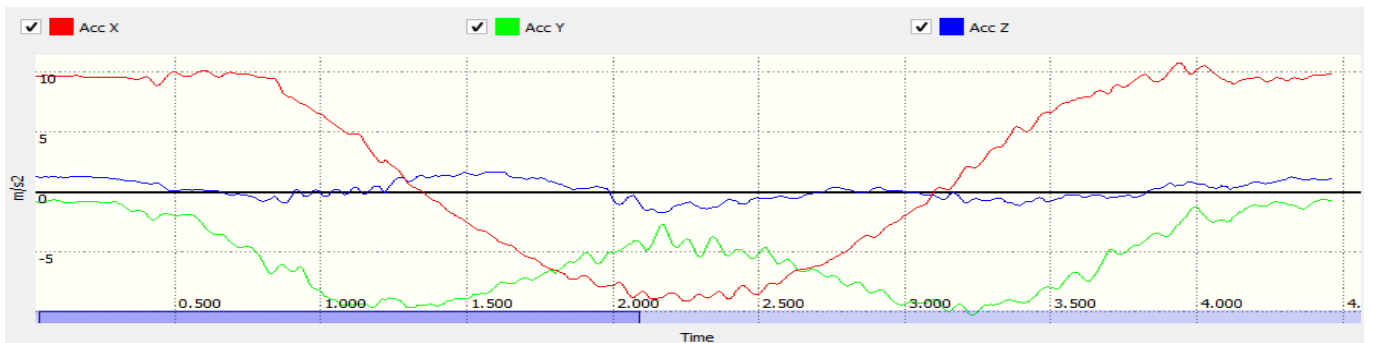


(a) Sensor 1

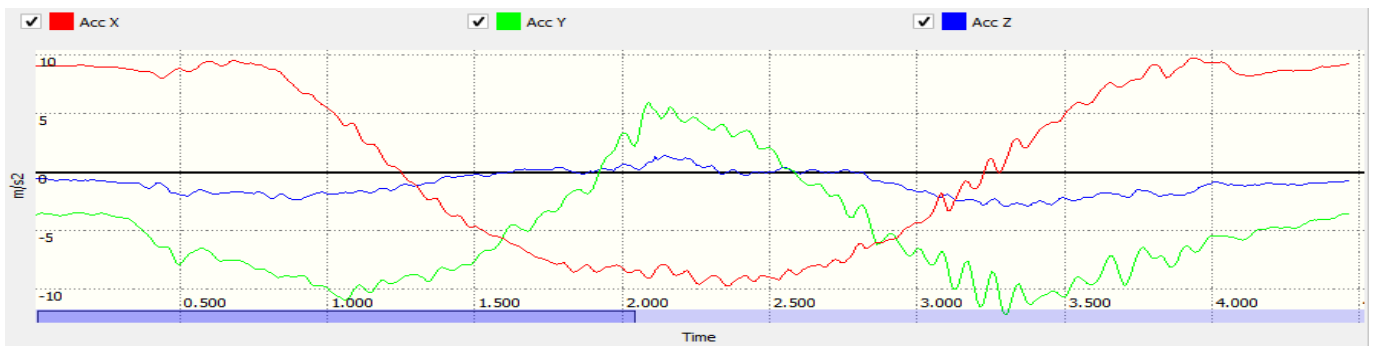


(b) Sensor 2

Figure 5. Acceleration Waveforms for Arm Extension

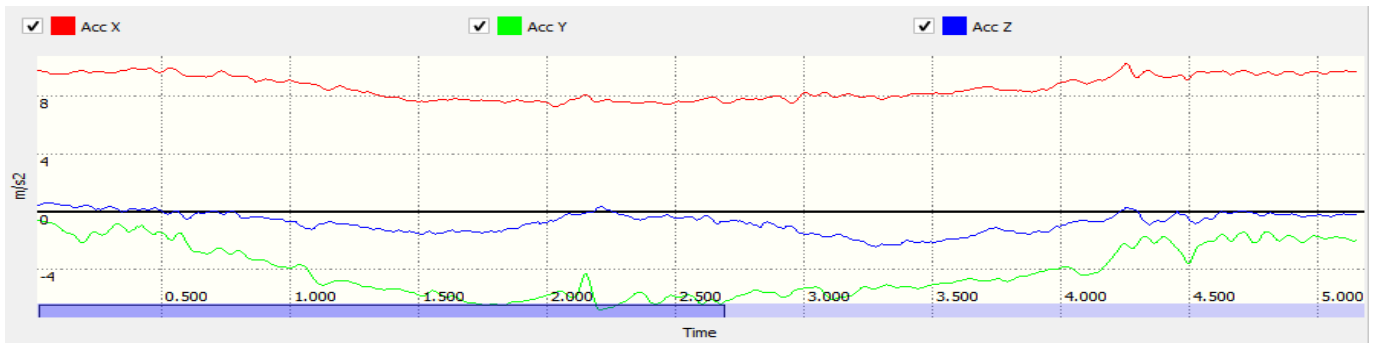


(a) Sensor 1

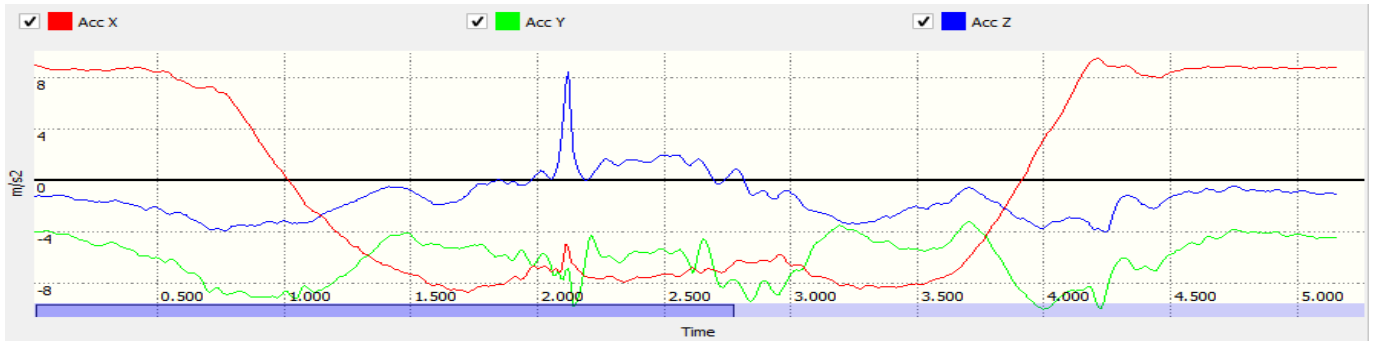


(b) Sensor 2

Figure 6. Acceleration Waveforms for Arm Raise

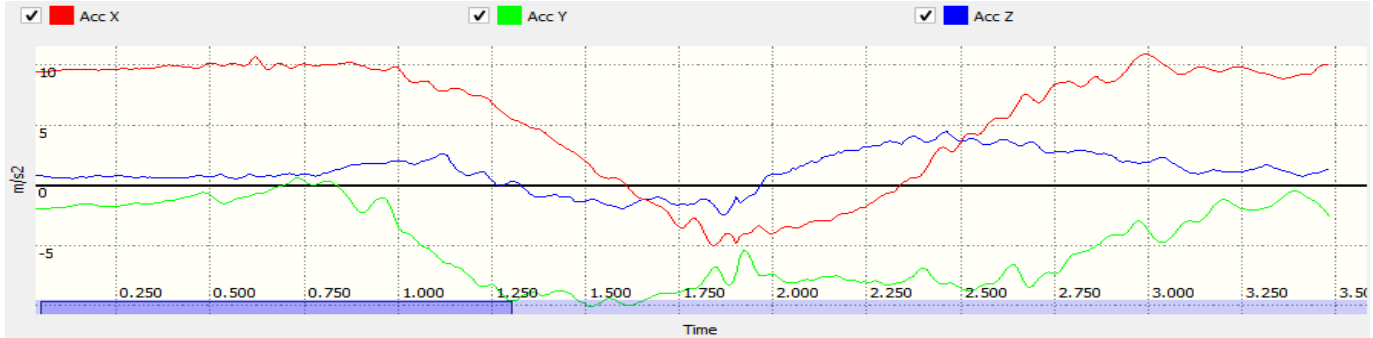


(a) Sensor 1

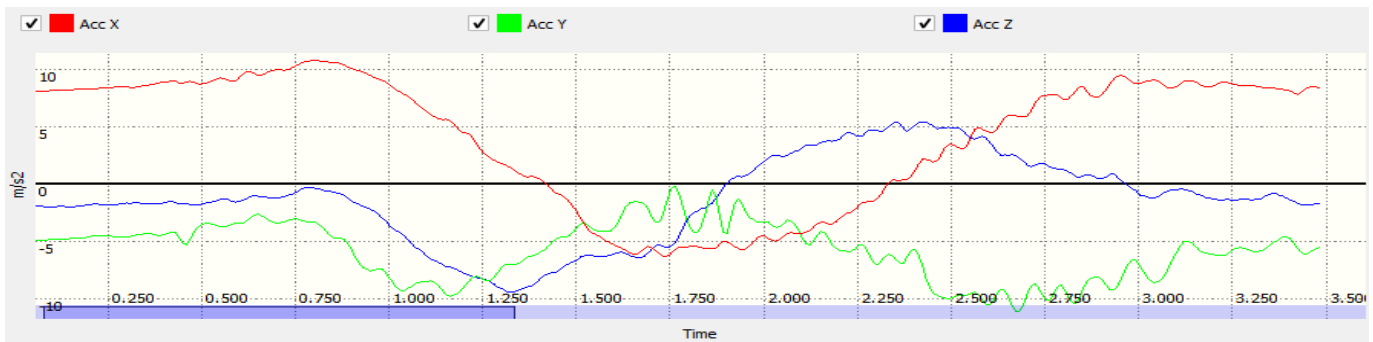


(b) Sensor 2

Figure 7. Acceleration Waveforms for Arm Raise Elbow Bend



(a) Sensor 1



(b) Sensor 2

Figure 8. Acceleration Waveforms for Clockwise Windmill

Motion 5: Counterclockwise Windmill. When performing the counterclockwise windmill from the initial position, the person rotates the shoulder 360 degrees counterclockwise and then returns to the initial position. Figure 9 shows the acceleration waveforms obtained during the counterclockwise windmill motion.

Motion 6: Shoulder Touch. When performing the shoulder touch movement from the initial position, the person bends the elbow until the hand touches the shoulder and then returns to the initial position. Figure 10 shows the acceleration waveforms obtained during the shoulder touch motion.

Motion 7: Side Arm Raise. When performing the side arm raise from the initial position, the person lifts the arm straight from the side 90 degrees until it is parallel to the floor, then returns to the initial position. Figure 11 shows the acceleration waveforms obtained during the side arm raise motion.

Motion 8: Wipe Right. When performing the wipe right movement from the initial position, the person bends the elbow until the arm is parallel to the floor, then rotates the forearm to the right as far as possible and then returns to the initial position. Figure 12 shows the acceleration waveforms obtained during the wipe right motion.

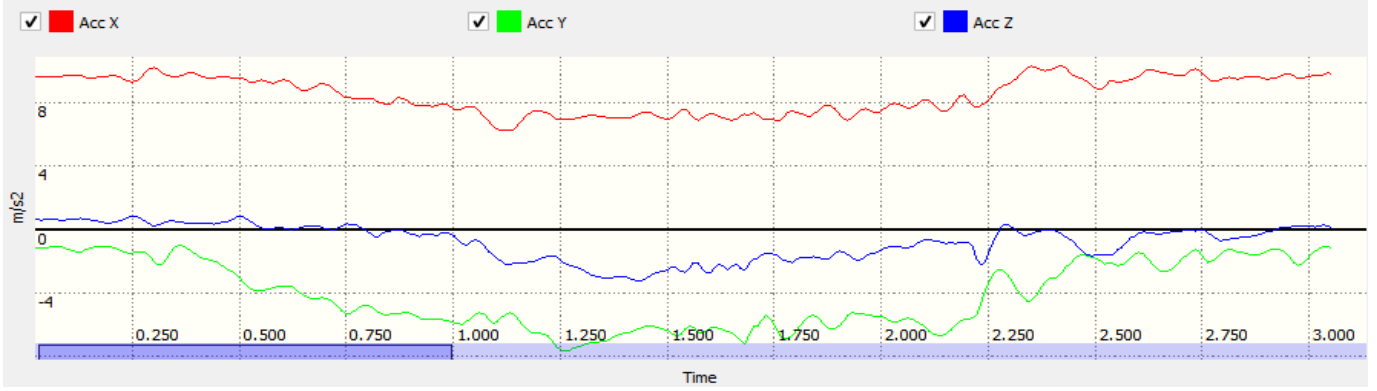
Motion 9: Wrist Rotation. When performing the wrist rotation from the initial position, the person bends the elbow until parallel to the floor, rotates the wrist inward and back again, and then returns to the initial position.

Artificial Neural Network

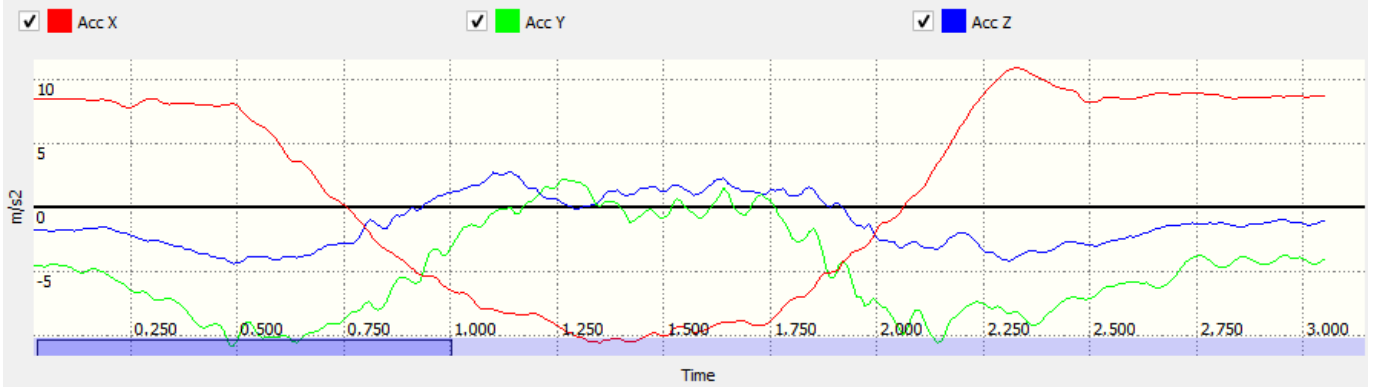
The robotic arm's controller had to be trained to distinguish among the arm's various movements. To make this possible, an ANN was used as a classifier to identify the specific arm movement to perform. The ANN was trained using the backpropagation algorithm and the triaxle accel-



Figure 9. Acceleration Waveforms for Counterclockwise Windmill



(a) Sensor 1



(b) Sensor 2

Figure 10. Acceleration Waveforms for Shoulder Touch

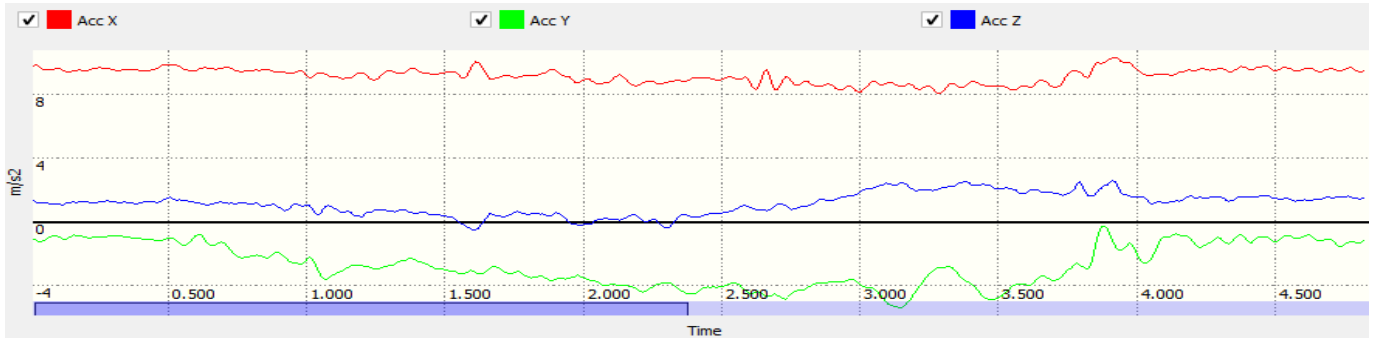
ation sampling data obtained from the IMUs. There was a total of 20 data sets for each motion. As mentioned previously, the IMU sampling rate was 100 Hz and each arm motion took approximately 3 to 5 seconds to complete. Each data-capture trial contained hundreds of individual data points. To reduce the size of the data sets, and be able to utilize the sets to train the ANN, the data sets were condensed into two statistical measurements for each sensor: the average rectified value (ARV) that can be calculated using Equation (1), and the root mean square (RMS) value, that can be calculated using Equation (2). The ARV is the average of the absolute values in the data set, whereas the RMS is the square root of the average. This would create a characteristic value that could be used as an input for the ANN.

$$x_{ARV} = \frac{1}{n} (|x_1| + |x_2| + \dots + |x_n|) \quad (1)$$

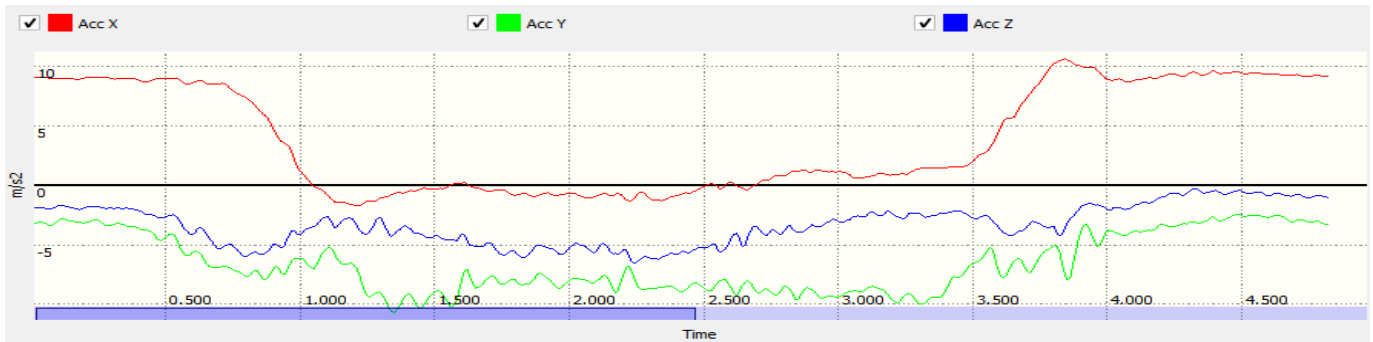
$$x_{RMS} = \sqrt{\frac{1}{n} (x_1^2 + x_2^2 + \dots + x_n^2)} \quad (2)$$

The size of the final training matrix was 12x265. This corresponds to having 12 input nodes that are signals coming from the X-Acc, Y-Acc, Z-Acc coordinates, from sensor 1 and sensor 2, each having the computed ARV and RMS values (3x2x2). The length of each vector was 265 samples; this was selected by looking at the 3-5 second signals and selecting enough samples to have reliable information from the IMU. A target set matrix (output) with 9 rows by 265 columns was constructed to train the ANN with the correct output values that should be learned. Each of the 9 rows corresponded to a particular motion, while the length of the matrix mirrored the training set. Each movement's row had a 1 in its output cell, if the current trail matched, otherwise it had a 0.

The data set was divided into three batches: training, validation, and testing. During the training stage, the network ran through epochs, or iterations, and attempted to minimize the error until it could not progress further. The training set used 70% of the total database, 20% for the validation process, and 10% for the testing stage.

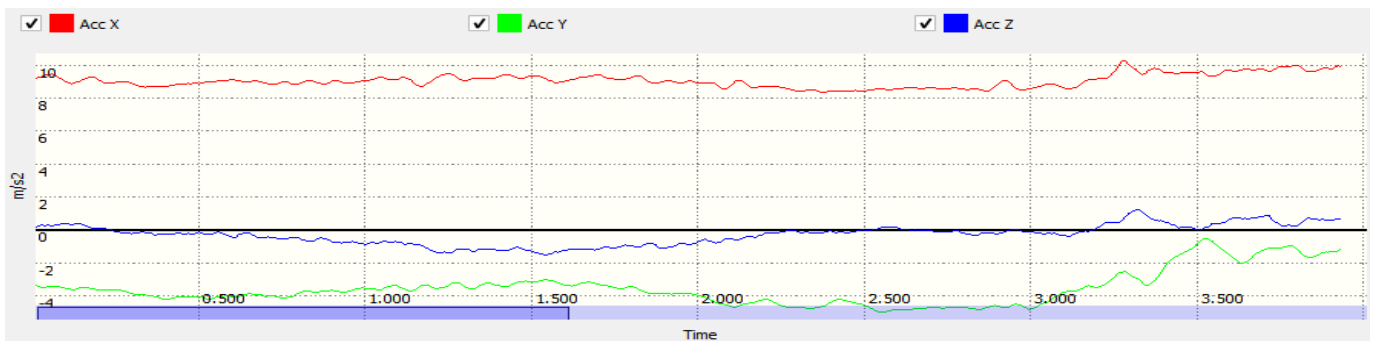


(a) Sensor 1

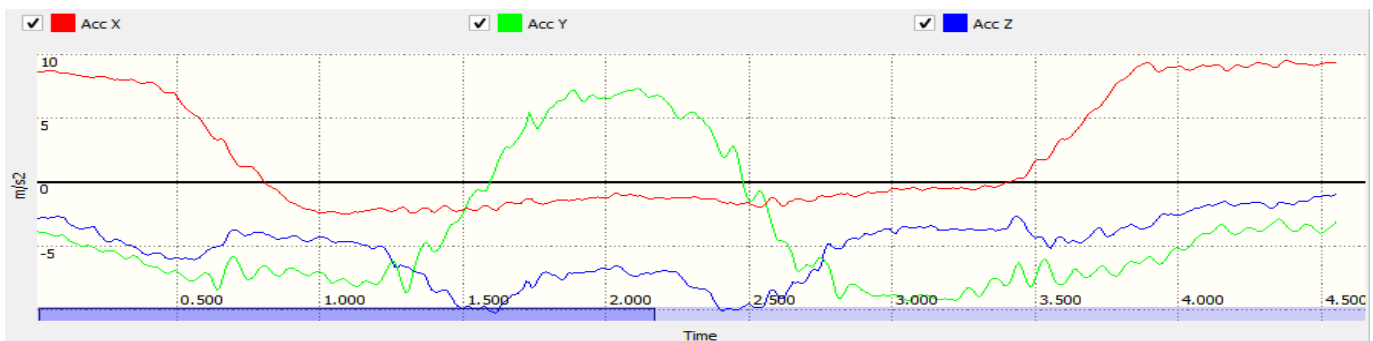


(b) Sensor 2

Figure 11. Acceleration Waveforms for Side Arm Raise



(a) Sensor 1



(b) Sensor 2

Figure 12. Acceleration Waveforms for Wipe Right

The validation stage was used to test the network progress, and signal when to stop the training, while the testing stage was used to measure the accuracy of the trained network. The database for the construction of the ANN consisted of 180 arm movements collected from four different subjects. Each subject performed each motion five times. The network architecture was constructed by selecting the amount of hidden neurons to place in the hidden layer of the network. This number can be tuned, but the general rule of thumb that was followed was to select a number somewhere between the number of inputs and outputs. For this study, there were 12 inputs and 9 outputs, so 10 neurons were placed in the hidden layer. The ANN was trained until the mean squared error of the output vector was minimized.

Robotic Arm

Figure 2 shows that the robotic arm used in this study had six degrees of freedom and used seven servo motors. Each servo had an individual signal port, with the exception of the two shoulder joint servos, which were driven in tandem. The six servos controlled base rotation, shoulder rotation, elbow rotation, wrists rotation, wrist pitch, and grabber. Initially, a separate program was developed to model the desired movements using user-input angle writes. This allowed the authors to see how the arm would need to move in order to execute the proper movement. The robotic arm was programmed to receive input voltages (PWM signal) to each servo, corresponding to the particular motion classified by the ANN system. Then the robotic arm executed the movements in a predetermined sequence when the commanded motion had been completed: the robotic arm paused for about 5 seconds and then returned to the starting position.

The movements were set up so that the motors were stepped through a range of angles until reaching the desired position. This was accomplished using “for loops” and time delays to make the movements smooth rather than abrupt. The implementation of the ANN was performed using the ANN toolbox from Matlab. Once the ANN identified the specific arm movement, it would automatically transition to a program in which each servo motor was assigned a corresponding control signal (PWM). This was possible by interfacing the computer running the Matlab software with an Arduino microcontroller.

Testing the Arm Extension Motion

The robotic arm was capable of mimicking the motions of a human arm in real time. As an example, consider the arm extension motion, which entails bending the elbow until the arm is parallel to the floor, then extending the arm all the

way forward. Figure 13 shows the initial position, then the subject begins to bend his/her elbow until the arm is parallel to the floor, as shown in Figure 14.



Figure 13. Subject in Initial Position



Figure 14. User Bends Elbow until Parallel to the Floor

Figure 15 shows that, after the person’s elbow is parallel with the floor, he/she then begins to slowly extend the arm until it is fully extended, as shown in Figure 16. While the person performs these movements, the XYZ acceleration data are acquired and imported into Matlab, which computes the RMS and ARV values for each coordinate. This information is then fed into the ANN. The network outputs the corresponding commands that the robotic arm should do to perform the arm extension movements.

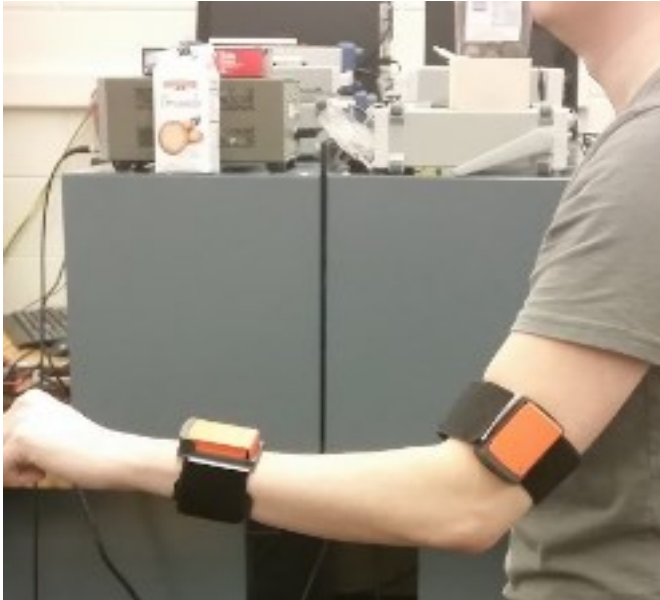


Figure 15. User Slowly Begins to Extend Arm

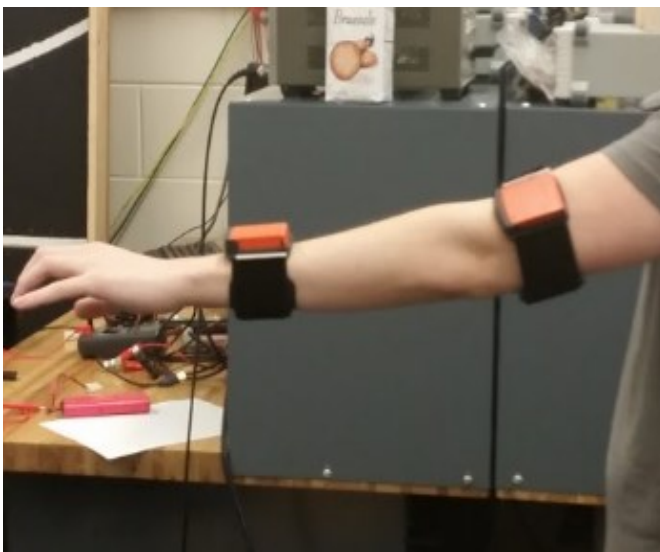


Figure 16. User Extends Arm

When the robotic arm is powered up, the arm assumes the initial position shown in Figure 17, and holds it until further input is received. Figures 18-20 show the corresponding arm extension motions performed by the robotic arm, mimicking the human arm movement described above. In particular for the arm extension motion, Figure 17 shows the robotic arm at the initial position that corresponds to a position of 10 degrees on the shoulder's servo motor, and 180 degrees angle on the elbow's servo motor. Then, the robotic arm begins to bend the elbow's joint until parallel to the floor (90 degrees on the elbow's servo motor), as shown in Figure 18.

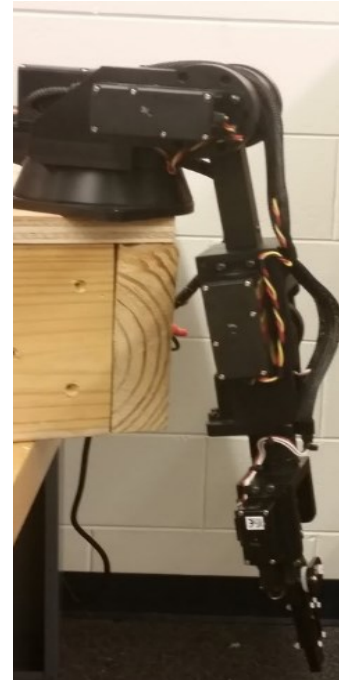


Figure 17. Robotic Arm in Initial Position



Figure 18. Robotic Arm Bends Elbow until Parallel to the Floor

Figure 19 shows that, after the robotic arm is parallel to the floor, it begins to extend itself by moving the shoulder's servo approximately 55 degrees. Figure 20 shows that, as the arm extends the angles for the shoulder and elbow joints, they have to be adjusted so that the arm maintains a horizontal position with reference to the floor. Once the robotic arm has performed the complete set of movements for the arm extension motion, the robotic arm returns to the initial position and waits for the next command.



Figure 19. Robotic Arm Slowly Begins to Extend Its Arm



Figure 20. Robotic Arm Fully Extended

Results

To determine the accuracy of the ANN classification system, an independent volunteer was asked to perform each of the nine motions. The accuracy of the classification was 88.8% (one motion was misclassified by the ANN). Due to the mechanical limitations of the robotic arm used in this study, not all of the nine motions were able to be performed exactly as originally intended. The main reason for this was that the robotic arm was designed to be mounted and operate in a horizontal position, as shown in Figure 20. Thus, in order to better mimic human arm movements, it would be necessary to use a robotic arm that can be mounted and operate in a vertical position. Due to this limitation, there were three human arm movements that the robotic arm was not able to perform exactly, namely: the wipe right, the counter-clockwise windmill, and the clockwise windmill.

Conclusions

The overall system was able to perform the commanded movements in real time, with a small delay of about three seconds, due to the signal processing time required on the computer. This delay can be reduced by interfacing the Xsens Technologies' software directly with Matlab, so that the intermediate step of importing the signals captured by the Xsens technology into an Excel spreadsheet is removed. The robotic arm mimicking system was successful, but currently unilateral. The ANN performed very well. In the test with the independent subject, the ANN was able to correctly identify eight of the nine motions (88.8%). This accuracy can be improved by expanding the database that was used to train, validate, and test the ANN. Only motions from four subjects were used to train, validate, and test the ANN, and motions from a fifth subject were used as independent motions to compute the accuracy of the system. Currently the system is unilateral; that is, the human subject is the one that sends signals to the robot. Adding haptic feedback, however, the robotic arm would be able to send signals to the human subject, making a bilateral system that could expand the possible applications.

Potential applications of robotic mimicking include the manufacturing and medical industries. Manufacturing companies can use such a system in a way that a person can teach a robotic structure specific actions to perform without having an expert programmer. Robotic limbs can be integrated with this system to help amputees or people with disabilities, so that this system can help these individuals in providing arm movements or improve physical therapy and the improvement of motor skills.

References

- [1] Lobov, S., Mironov, V., Kastalskiy, I., & Kazantsev, V. (2015). Combined Use of Command-Proportional Control of External Robotic Devices Based on Electromyography Signals. *Medical Technologies in Medicine*, 7(4), 30-37.
- [2] Hickman, S., Mirzakhani, A., Pabon, J., & Alba-Flores, R. (2015). A Case Study on Tuning Artificial Neural Networks to Recognize Signal Patterns of Hand Motions. *Proceedings of the IEEE SoutheastCon*, (pp. 1-4). Fort Lauderdale, FL. DOI: 10.1109/SECON.2015.7132893
- [3] Sekhar, R., Musalay, R., Krishnamurthy, Y., & Shreenivas, B. (2012). Inertial Sensor Based Wireless Control of a Robotic Arm. *IEEE International Conference on Emerging Signal Processing Applications*, (pp. 87-90). Las Vegas, NV. DOI: 10.1109/ESPA.2012.6152452

-
- [4] Georgi, M., Amma, C., & Schultz, T. (2015). Recognizing Hand and Finger Gestures with IMU based Motion and EMG based Muscle Activity Sensing. *Proceedings of the International Conference on Bio-inspired Systems and Signal Processing*, (pp. 99-108). Lisbon, Portugal. DOI: 10.5220/0005276900990108
- [5] Jung, P., Lim, G., Kim, S., & Kong, K. (2015). A Wearable Gesture Recognition Device for Detecting Muscular Activities Based on Air-Pressure Sensors. *IEEE Transactions on Industrial Informatics*, 11(2), 485-494.
- [6] Malegam, M., & D'Silva, M. (2011). Mimicking Robotic Hand-Arm, *Annual IEEE India Conference*, (pp. 1-5). Hyderabad, India. DOI: 10.1109/INDCON.2011.6139365
- [7] Wireless Motion Tracker XSENS. (n.d.). Retrieved from <https://www.xsens.com/products/mtw-development-kit>
- [8] Ripley, B. D. (1996). *Pattern Recognition and Neural Networks*, Cambridge University Press.
- [9] Stergiou, C., & Siganos, D. (1996). Neural Networks. Retrieved from http://www.doc.ic.ac.uk/~nd/surprise_96/journal/vol4/cs11/report.html
- [10] Shiffman, D. (2017). The Nature of Code: Chapter 10. Neural Networks. Retrieved from <http://natureofcode.com/book/chapter-10-neural-networks/>
- [11] Artificial Neural Networks Technology, University of Toronto, Department of Psychology. (n.d.). Retrieved from <http://www.psych.utoronto.ca/users/reingold/courses/ai/cache/neural2.htm>
- [12] XBee Pro, 2.4GHz, XBee 802.15.4 RF modules from Digi. (n.d.). Retrieved from http://www.digi.com/pdf/ds_xbeemultipointmodules.pdf
- [13] Arduino Mega Microcontroller. (n.d.). Retrieved from <https://www.arduino.cc/en/Main/arduinoBoardMega>

IMANI AUGUSMA is a graduate student in the Master of Science in Applied Engineering Program at Georgia Southern University. Her areas of interest include intelligent vehicles, mechatronics, and engines. Ms. Augusma may be reached at ia00336@georgiasouthern.edu

Biographies

FERNANDO RIOS is an associate professor in the Electrical Engineering Department at Georgia Southern University. His areas of research include robotics, neural networks, fuzzy logic, and embedded systems. He has over 20 years of experience in higher education. Dr. Rios may be reached at frios@georgiasouthern.edu

ROCIO ALBA-FLORES is an associate professor in the Electrical Engineering Department at Georgia Southern University. Her areas of research include control systems, biomedical applications, and robotics. Dr. Alba has over 20 years of experience in higher education. Dr. Alba may be reached at ralba@georgiasouthern.edu

COMPARATIVE STUDY IN THE OPTIMAL DESIGN OF CUSTOM-CONSTRUCTED WIND AUGMENTATION SHROUDS

Ulan Dakeev, Texas A&M University-Kingsville; Farzin Heidari, Texas A&M University-Kingsville;
Mohammad Mustaq Bijapur, Texas A&M University-Kingsville; Sumanth Yanamala, Texas A&M University-Kingsville

Abstract

In this study, the authors evaluated the impact of wind velocities on power generation, and how wind energy depends on various flow behaviors subject to the medium through which the wind flows. The last two decades have seen rapid growth and improvement in using wind energy to produce electricity, due to concerns relating to global warming and the continuous increase in the price of fossil fuels [1]. Wind power produced increments by a variable of eight when the wind pace was multiplied, which demonstrated that energy available in the wind directly reflects its power [2]. The measure of producible wind is given by $p = 0.5\rho AV^3$, which demonstrates that wind power is largely impacted by speed, specifically the solid shape of wind speed. Previous studies have successfully revealed that, for constant wind available, the shroud with an inlet angle of 30° delivers maximum energy among three different shrouds with inlet angles of 20°, 25°, and 30° [3]. To extend previous research, the authors of this current study tested three distinct covers with differing delta edges of 20°, 30°, and 35°, using IBM SPSS Statistics 22. The goal was to determine the ideal configuration of the cover producing the most wind energy. Results indicated that, for constant wind, the shroud (cover) with an inlet angle of 35° delivered the maximum wind energy among the three different shrouds with inlet angles of 20°, 30°, and 35°. Therefore, this shroud represented the optimal design for achieving maximum wind energy.

Introduction

Wind is one of the consistent and accessible energy sources. The world is experiencing an excessive demand for energy, due to rapid economic growth and industrialization [4]. There has been a huge increase in the consumption of fossil fuels to produce energy. The global carbon dioxide content has grown from 280 ppm in the pre-industrial era to 400 ppm in May of 2013, a 39% increase in carbon dioxide emissions. Recent reports released by the National Oceanic and Atmospheric Administration (NOAA) [5] indicate that global CO₂ content was 399.29 ppm in January of 2015, and had increased to 402.59 ppm by January of 2016. Consider-

ing the negative effects of fossil fuels emitting CO₂ and harmful gasses, the continuous increase in the price of fossil fuels, and heavy consumption leading to depletion of resources for future generations, most parts of the world have shown a keen interest in wind energy technologies to produce power [6].

The wind and its abundant nature are attractive as a viable source for electricity generation [7]. The power output a wind turbine can deliver depends on wind velocity, which is responsible for rotating the blades that convert mechanical energy into electrical energy. In this study, the authors explored the effects of wind velocity on the newly augmented shroud devices with varying inlet angles of 20°, 30°, and 35°, designed to maximize wind velocities.

Literature review

Global warming is one of the major threats to the world that everyone should be aware of; we all should act responsibly to control and reduce its future effects. About 80% of global warming results from CO₂ emissions from fossil fuels [8]. Wind power has the ability to stop this potential environmental disaster, as it is pollution free and consumes virtually no water to generate electricity, thus reducing CO₂ emissions [9]. Recent reports indicate an expansion in worldwide wind power limits of 318 GW from 39 GW between 2003 and 2013. On May 11, 2014, at around 1:00 pm, Germany recorded 21.3 GW of wind power capacity, outpacing solar power, which was 15.2 GW. The increase indicates that wind power has the capability of being one of the best resources for generating electricity [10].

The wind turbine is utilized as the main source of transforming wind energy into electrical energy [11]. Wind turbines are usually categorized as horizontal or vertical axis, based on design, and as offshore or onshore, based on the installed location. Power capacity of a wind turbine generally depends on design and wind speed [12]. One major drawback of wind turbine technology is with low wind speeds possessing less energy density per volume of air hitting turbine blades, which increases production costs compared to fossil fuels [13]. Various studies conducted to improve the

energy density of wind have shown that concentrator augmented wind turbines would be one of the best ways to improve power capacity and make it more cost effective [14]. To enhance the power capacity of a wind turbine, the authors of this current study have developed three distinct shrouds with inlet angles of 20°, 30°, and 35°, and used in such a way as to enhance the wind speed, which eventually builds the wind power capacity of a turbine.

Methodology

To develop a new technique to improve the power efficiency of a wind turbine, the authors of this study designed and 3D printed three different shrouds with inlet angles of 20°, 30°, and 35° for the tests. The dimensions of the shrouds were designed to produce maximum wind output from the available wind and achieve optimal design. This project involved three different tools: PTC Creo3.0 for designing, Cube Pro for 3D printing, and IBM SPSS for data analysis. Figure 1 shows three 3D printed shrouds attached to cylindrically shaped sheet metal.



Figure 1. 3D-Printed Shrouds

To generate the wind required for the experiment, a 7-inch-diameter blower was used, and the experiment was conducted in a closed environment to avoid any fluctuations in wind direction and velocity. Figure 2 shows the 35° shroud being measured for wind velocity. Using anemometers, 30 different readings of wind velocities were collected at both the inlet and outlet.



Figure 2. Shroud with 35° Inlet Angle

The authors repeated the procedure and collected data from the 20° and 30° shrouds. They then performed a statistical analysis, using one-way ANOVA, to examine the collected data and determine any significant differences between the shrouds.

Data Analysis

A one-way ANOVA test in SPSS Statistics 22 was performed to analyze and compare the differences between the inlet and output velocities of different shrouds. Table 1 presents the descriptive data of the shroud velocities. The mean value column shows that the mean velocity for constant inlet ($\mu=22.227$) was higher for the shroud with an inlet angle of 35° ($N=30$, $\mu=28.211$), when compared with the other shrouds with inlet angles of 20° ($N=30$, $\mu=25.751$) and 30° ($N=30$, $\mu=25.816$). This signifies that the 35° shroud achieved higher efficiency in producing greater output velocity from available constant inlet velocity.

Table 2 presents the ANOVA test data. The p-value was $0.00(<0.05)$, indicating a significant difference between the output velocities produced by the three custom-constructed shrouds for the constant input velocity.

The Tukey test data in Table 3 reveal a maximum mean difference value ($M.D = 5.983$) between the inlet and output velocities for the 35° shroud. The statistics show that this shroud has the ability to achieve maximum efficiency to produce greater output velocity from a constant input velocity, when compared with the 20° and 30° shrouds (see again Tables 1 and 2).

Table 1. Descriptive Statistics: Incoming versus Outgoing Wind Velocity

Velocity Type	N	Mean	Std. Deviation	Std. Error	95% Confidence Interval for Mean	Minimum	Maximum	
					Lower Bound	Upper Bound		
Inlet velocity	30	22.23	1.91	0.35	21.52	22.94	17.77	27.42
20° Outlet Velocity	30	25.75	1.87	0.34	25.05	26.45	21.87	30.82
30° Outlet Velocity	30	25.82	1.91	0.35	25.10	26.53	22.30	33.37
35° Outlet Velocity	30	28.21	3.62	0.66	26.86	29.56	23.36	40.59
Total	120	25.50	3.23	0.29	24.92	26.08	17.77	40.59

Table 2. SPSS ANOVA Output: Inlet versus Outlet Wind Velocity

Velocity Type	Sum of Squares	Df	Mean Square	F	Sig.
Between Groups	546.6	3.0	182.2	30.5	0.0
Within Groups	692.3	116.0	6.0		
Total	1238.9	119.0			

Table 3. Post Hoc Test

	Dependent variable	Velocity Type	Mean Difference (I-J)	Std. Error	Sig.	95% Confidence Interval	
						Lower Bound	Upper Bound
Tukey HSD	Inlet velocity	20° Outlet Velocity	-3.52400*	.631	.00	-5.17	-1.88
		30° Outlet Velocity	-3.58867*	.631	.00	-5.23	-1.94
		35° Outlet Velocity	-5.98333*	.631	.00	-7.63	-4.34
	20° Outlet Velocity	Inlet velocity	3.52400*	.631	.00	1.88	5.17
		30° Outlet Velocity	-.06467	.631	.00	-1.71	1.58
		35° Outlet Velocity	-2.45933*	.631	.00	-4.10	-0.82
	30° Outlet Velocity	Inlet velocity	3.58867*	.631	.00	1.94	5.23
		20° Outlet Velocity	.06467	.631	.00	-1.58	1.71
		35° Outlet Velocity	-2.39467*	.631	.00	-4.04	-0.75
	35° Outlet Velocity	Inlet velocity	5.98333*	.631	.00	4.34	7.63
		20° Outlet Velocity	2.45933*	.631	.00	0.82	4.10
		30° Outlet Velocity	2.39467*	.631	.00	0.75	4.04

Conclusion

The motivation behind this study was to examine the ideal design for uniquely built wind augmentation devices. The authors developed three designs with various inlet angles of 20°, 30°, and 35° for comparing wind flow efficiency. The one-way ANOVA test results showed that the 35° shroud amplified wind velocity significantly, compared to the inlet wind velocity of the shroud. Moreover, this shroud was the most efficient with the highest mean values of wind speeds at the exit. In terms of efficiency of velocities at the exit, the 35° shroud followed the 30° and 20° shrouds.

References

- [1] Lu, M.-S., Chang, C.-L., Lee, W.-J., & Wang, L. (2008). Combining the wind power generation system with energy storage equipment. *Proceedings of the IEEE Industry Applications Society Annual Meeting*. Edmonton, Alberta, Canada. doi:10.1109/08IAS.2008.139
- [2] Dakeev, U. (2016). Comparative study of custom-constructed wind augmentation shrouds on a small-scale wind turbine. *Proceedings of the ASEE Annual Conference*. New Orleans, LA.
- [3] Iowa Energy Center. (2016). *Wind speed and power*. Retrieved from <http://www.iowaenergycenter.org/wind-energy-manual/wind-and-wind-power/wind-speed-and-power>
- [4] Leung, D. Y. C., Caramanna, G., & Mercedes Maroto-Valer, M. (2014). An overview of current status of carbon dioxide capture and storage technologies *Renewable and Sustainable Energy Reviews*, 39(11), 426-443. doi: 10.1016/j.rser.2014.07.093
- [5] NOAA. (2013). Retrieved from <http://www.esrl.noaa.gov/gmd/ccgg/trends>
- [6] Xu, J., Li, L., & Zheng, B. (2016, June). Wind energy generation technological paradigm diffusion. *Renewable and Sustainable Energy Reviews*, 59, 436-449. doi: 10.1016/j.rser.2015.12.271
- [7] Snellin, D. (2009, Fall). *Wind power: Harnessing the wind as a sustainable source of energy*. Retrieved from <http://www2.hawaii.edu/~dsnellin/100/Researchpaper.html>
- [8] Afnan Mahmood Freije, A. M., Hussain, T., & Salman, E. A. (2016, March 22). Global warming awareness among the University of Bahrain science students. *Journal of the Association of Arab Universities for Basic and Applied Sciences*. doi: 10.1016/j.jaubas.2016.02.002
- [9] Global Wind Energy Council. (2014). *Global statistics*. Retrieved from <http://www.gwec.net/global-figures/graphs>
- [10] Morris, C. (2014, May 13). *German power prices negative over the weekend*. Retrieved from <http://energytransition.de/2014/05/german-power-prices-negative-over-weekend/>
- [11] Liu, W. (2016). Design and kinetic analysis of wind turbine blade-hub-tower coupled system. *Renewable Energy*, 94, 547-557. doi: 10.1016/j.renene.2016.03.068
- [12] Ojosu, J. O., & Salawu, R. I. (1990, January). An evaluation of wind energy potential as a power generation source in Nigeria. *Solar and Wind Technology*, 7(6), 663-673. doi: 10.1016/0741-983X(90)90041-Y
- [13] Phillips, D. G. (2003). *An investigation on diffuser augmented wind turbine design*. (Unpublished doctoral dissertation). The University of Auckland, Auckland, New Zealand.
- [14] Shonhiwa, C., & Makaka, G. (2016). Concentrator augmented wind turbines: A review. *Renewable and Sustainable Energy Reviews*, 59, 1415-1418. doi: 10.1016/j.rser.2016.01.067

Biographies

ULAN DAKKEEV is an assistant professor in the Industrial Technology Department in the College of Engineering, Texas A&M University-Kingsville. His areas of research include renewable energy (wind energy), quality in higher education, motivation, and engagement of students. Dr. Dakeev may be reached at Ulan.dakeev@tamuk.edu

FARZIN HEIDARI currently serves as Associate Professor of Industrial Management and Technology at Texas A&M University-Kingsville. Dr. Heidari has 26 years of experience in manufacturing and CAD/CAM/CNC courses. He currently serves as the graduate coordinator for the Industrial Management program. Dr. Heidari may be reached at farzin.heidari@tamuk.edu

BIJAPUR MOHAMMAD MUSTAQ is currently pursuing a master's degree from Texas A&M University-Kingsville in the Department of Industrial Management and Technology. Having his undergraduate degree in mechanical engineering from Jawaharlal Nehru Technological University, strong determination and curiosity in learning new technologies paved a path for his immense interest in research and development in the areas of engineering. His present role as a graduate research assistant in the Department of Industrial Management and Technology at Texas A&M University-Kingsville provides an opportunity to do research in the areas of renewable energy and best optimal wind turbine technologies for power generation. Mr. Mustaq may be reached at mohammad.bijapur@students.tamuk.edu

SUMANTH YANAMALA is currently a graduate teaching assistant for Industrial Management and Technology at Texas A&M University-Kingsville. He earned his BE degree in Civil Engineering from Jawaharlal Nehru Technological University, Hyderabad, India. His interests include renewable energy, wind energy, and sustainability. Mr. Yanamala may be reached at su-manth.yanamala@students.tamuk.edu

THERMAL PERFORMANCE OF RECYCLED AGGREGATE USING BUILDING ENERGY SIMULATION PROGRAMS

Thomas Nicholas, The University of North Carolina at Charlotte; Tara Cavalline, The University of North Carolina at Charlotte; Dixie Johnson, The University of North Carolina at Charlotte; Morgan Laney, The University of North Carolina at Charlotte

Abstract

As the building industry in the U.S. rapidly expands, the reuse of recycled demolition waste as aggregates is becoming increasingly more common and more urgent. The constant use of raw virgin aggregate is resulting in the depletion of resources, a lack of space for landfills, increasing costs, and heightened levels of environmental impact. The focus of this study was on the effects of using recycled demolition waste aggregates and their corresponding measured thermal properties, including specific heat capacity and thermal conductivity, in masonry mortar applications. The new types of aggregate were analyzed for efficiency and practical utilization in construction in seven locations across the U.S. by embedding the recycled material into the building envelope of a strip mall mercantile build model from the National Renewable Energy Laboratory in the EnergyPlus Building Energy Simulation Program. Thermal efficiency for the utilization of recycled brick masonry aggregate (RBMA) in lightweight masonry construction was modeled for various U.S. climate zones, and its efficiency in each zone was compared to typical steel and masonry construction types. An energy consumption analysis was performed for a baseline steel-framed strip mall. The results were compared to energy-consumption analysis results for: 1) a fully grouted, lightweight masonry wall containing mortar that used normal sand for aggregates (C144 mortar); 2) a fully grouted, lightweight masonry wall that used mortar containing RBMA; and, 3) a fully grouted, lightweight masonry wall that used mortar containing lightweight, expanded slate aggregate. After comparing each of the strip mall construction types, it was determined that the RBMA mortar mixtures performed as well as or better than the C144 mortar mixtures. However, the baseline steel strip mall outperformed the masonry strip mall at several locations. Opportunities for future research in RBMA mortar mixtures exist in a regional analysis, a regional recycled aggregate cost analysis, and a lifecycle cost analysis.

Introduction

Research is being conducted in many areas in order to improve the design and construction of infrastructure and facilities and reduce the environmental impact and energy

consumption from the construction phase through the complete service life. A key material used in many facets of the built environment are aggregates. According to Gilpin et al. [1], approximately 2.7 billion metric tons of aggregates per year were used in the U.S. Of those 2.7 billion metric tons of aggregate, pavement accounted for 10-15%, general road construction and maintenance accounted for 20-30%, with the remaining 60-70% going to structural concrete. Recent statistics have indicated that the estimated global consumption of aggregates in construction reached 26 billion tons per year worldwide by 2012 [2], with the demand doubling over the next 20 to 30 years [3]. To alleviate the strain on the environment and on the natural resources associated with this demand for aggregates, recycled aggregates have become an increasingly enticing option for stakeholders. Use of recycled aggregates, including those from construction and demolition (C&D) waste is a promising area for improving the sustainability of our built environment.

C&D waste is defined by the Environmental Protection Agency (EPA) as “the waste material produced in the process of construction, renovation, or demolition of structures,” [4], and can consist of a variety of materials, including crushed concrete, masonry, and pavement [5]. The composition of C&D waste is a function of both the source infrastructure material(s) as well as processing, handling, and stockpiling [6]. C&D waste has successfully been utilized in a number of structural applications [7-9]. However, recycling of C&D waste is not a widely accepted practice, due to stakeholder risk perception and a lack of certainty in the quality of the finished product. Factors such as low tipping fees for landfills also have a direct effect on how the construction industry and municipalities choose to dispose of waste [5], and local market factors can determine whether or not material is available for beneficial reuses in new infrastructure or facilities [10].

A number of studies have been conducted internationally on the use of municipal solid waste and C&D waste as aggregates in various applications, but very little research has been performed in this area in the U.S. Overall, the majority of the research performed on recycled aggregates has been in roadbeds and concrete applications [9, 11, 12]. Although a number of studies exist on reuse of recycled concrete aggregate in structural applications [6, 9, 13-17], less research

has been focused on masonry C&D waste as aggregates [6, 8, 9, 18-20]. Relatively little research has been conducted in the area of use of C&D waste as aggregates in mortar and grout applications [21], as will be detailed subsequently.

Before lightweight construction options became available, concrete masonry was the primary material used in building construction. Concrete masonry construction can provide significant benefits to owners, due to the fact that it is energy efficient, products can be locally produced, it includes materials of natural origins with long life expectancies, and can incorporate recycled materials [5]. The thickness and density of concrete masonry construction provide desirable thermal mass characteristics, facilitating the storage of heat. Concrete masonry materials also provide effective thermal storage, due to their high density and specific heat properties, ultimately allowing buildings to have reduced heat and cooling loads, decreased indoor temperature swings, and can shift loads to off-peak hours [22]. Substituting recycled aggregates for raw virgin aggregates in mortar and grout applications could allow buildings constructed with concrete block to be a more sustainable option than conventional masonry construction.

Many types of recycled materials have been studied for use in concrete and concrete masonry applications, but very few have been studied for reuse in concrete masonry mortar and grout [21]. Those that have been studied often have sufficient structural strength and are sustainable substitutes for natural sand mortars. Ledesma et al. [23] studied the use of fine recycled aggregate from concrete masonry waste. The recycled concrete masonry aggregate was obtained from a recycling plant that crushed and sieved, and reinforcing steel was removed from the aggregates before distribution. It was found that up to 40% of the natural sand could be replaced with the fine recycled aggregate; however, there were some negative effects. The fine recycled aggregate mortars stayed wet for a longer period of time. This was due to the inability of water to evaporate from the mortar. The final results indicated that there was no difference in structural strength between the natural sand mortar and the fine recycled aggregate.

In another study [24], the authors analyzed 100% replacement of the natural sand in the mortar mix with demolished houses. The demolition waste aggregate obtained from the houses consisted of ceramic, mortar, and concrete masonry. It was proven through testing that the recycled mortar variations performed as well as the natural sand mortars and often improved the mortar properties. Those same authors stated that “this improvement was due to both the adequate size grading distribution of the recycled aggregates and the low quality of natural aggregates located in Havana, Cuba.”

Despite the low quality of the natural aggregates, a more environmentally conscious substitute was found. In another study by Nicholas et al. [21], the authors demonstrated the compressive suitability of several masonry mortars that included recycled aggregates as well as C&D waste.

Thermal performance testing of masonry materials is often limited to measured properties of specific materials and conventional wall assemblies. ACI 122R-12 provides guidance on the thermal properties of concrete and masonry materials, including lightweight concrete, mortar, and brick [25]. Other published data in ACI 122-R12 have been prepared in order to provide thermal resistance values, thermal mass values, thermal lag values, and supporting computational methodologies for several of types of conventional masonry wall systems [25]. Tatro [26] provided a review of thermal properties for many materials potentially comprising recycled aggregates in ASTM STP 169D. However, although design values and computational guidance are presented in ACI 122 and ASTM STP 169D, values for recycled materials, often more porous than conventional materials due to the influence of adhered mortar [9], are not specifically provided. Overall, a review of the literature indicates that, by replacing the conventional aggregates used in mortar and grout applications, concrete masonry could be an effective option in sustainable building construction for reasons associated with both beneficial reuse and building energy savings. However, more research is needed, particularly in the building energy area, to validate the limited information available to support this potential recycling use.

Methodology

EnergyPlus is the U.S. Department of Energy’s (DOE) robust building energy simulation program (BESP). EnergyPlus was selected for a BESP investigation, due to its ability to comprehensively provide energy analyses and thermal load simulations [27]. Based on a building’s physical characteristics, EnergyPlus can calculate heating and cooling loads necessary to maintain ideal thermal control points, conditions through a secondary HVAC system and coil loads, and the energy demands of primary equipment. EnergyPlus models heating, cooling, lighting, ventilation, miscellaneous energy flows, and water use [27]. Another important feature of the program is its ability to factor in weather conditions. Weather data inputs include location, data source, latitude, longitude, time zone, elevation, peak heating and cooling design conditions, holidays, daylight savings periods, as well as typical and extreme periods. For the purposes of this current project, the OpenStudio Application Suite plug-in for Google SketchUp was used. OpenStudio Application Suite was designed by the National Renewable Energy Laboratory (NREL) and was programmed

around EnergyPlus in order to provide a supporting GUI interface for whole-building energy modeling simulations [28].

A standard U.S. DOE strip mall model was used to analyze the thermal performance of recycled aggregates in mortar applications in concrete masonry construction. To date, there are six mortar mix designs that have been tested for adequate compressive strength. Testing the compressive strength before obtaining thermal data ensured that the mix designs were adequate for structural use. The six types of aggregates used in the mortar mix designs were C144 (reference sand), expanded slate, DBS (demolition brick sand), DB2, DB3, and DB4. The DBS aggregates had bonding complications during prism testing, due to particle elongation preventing prescribed mortar joint height. As a result, a new DBS mortar mix was created and DB4 was selected due to its strength being the highest of the series.

Two mortar mixtures, C144 and DBS, were tested for thermal performance in Miami, FL, and Phoenix, AZ. Thermal performance testing included specific heat capacity and thermal conductivity. Of the two mortar mixtures, only the most adequate mixtures were selected to replace the C144 fine aggregate. Adequate recycled aggregate mortar models were considered to be models that performed as well as or better than the lightweight and normal-weight C144 mortar models. The U.S. DOE developed a database of sixteen commercial reference buildings across the U.S., which represent all U.S. climate zones and approximately 70% of the commercial building stock [29]. The reference model strip mall investigated in this study was a U.S. DOE benchmark strip mall new construction mercantile building. Figure 1 shows benchmark model proportions and store layout.

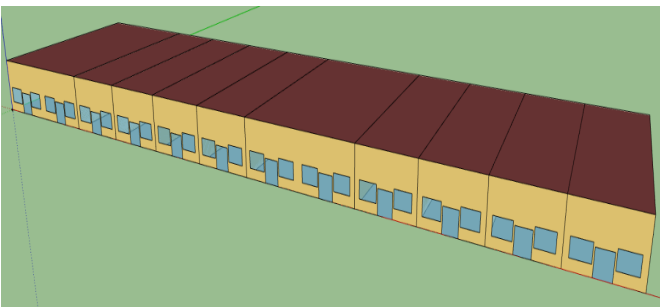


Figure 1. Solid DOE Benchmark Model—Exterior View

The building form required was a single story with an aspect ratio of 4.0 to 1.0 that housed ten stores with a total of 22,500 ft² (2090 m²); the floor-to-ceiling height was 17 ft (5.18m), and it had a glazing fraction of 0.11 [29]. The south-facing wall was the only glazed wall in the strip mall model, including glass doors and windows. The north-facing wall had typical exterior doors for rear store access.

Building envelope construction for the concrete masonry strip mall models included fully grouted concrete masonry walls, a built-up flat roof with insulation above deck, and a slab-on-grade floor. The building envelope construction complied with ASHRAE Standard 90.1-2004. Roof construction included a typical built-up roof with a roof membrane, non-resolution roof insulation, and metal decking. Creating a concrete masonry reference model in EnergyPlus using the strip mall reference model was the first step in inserting the recycled aggregate mortar materials. By creating a concrete masonry model based on the DOE reference model, accurate energy use values were generated.

The building envelope had to be changed from steel-framed to concrete-masonry with the EnergyPlus IDF Editor. The concrete-masonry material data were obtained from a predefined EnergyPlus IDF file with building materials from the ASHRAE 2005 Handbook—Fundamentals. The reference building exterior envelope from exterior to interior consisted of wood siding, steel-frame non-residential wall insulation, and ½-inch gypsum. Concrete masonry building envelope construction from exterior to interior consisted of 1 inch of stucco, 8-inch concrete block (lightweight and normal weight with C144 mortar), and ½-inch gypsum. A building envelope was created for lightweight and normal-weight concrete masonry construction using C144 mortar. The thermal performance data gathered for specific heat capacity and thermal conductivity for each mortar mix design were entered into an EnergyPlus strip mall model and compared to a typical U.S. benchmark model. A data-based analysis was then performed between the seven models and a conclusion was made based on whether the recycled aggregates used in the mortar mix design were comparable to those of virgin aggregates. The data analysis determined whether or not recycled aggregates are a more energy efficient option than raw virgin aggregates.

For this current investigation, a building energy simulation was performed in two of the eight climate zones across the U.S. The two building simulations were performed in Miami, FL, (Zone 1A) and Phoenix, AZ, (Zone 2B). These locations were recommended for energy simulation programs by the DOE, due to the overwhelming amount of options at these locations [30].

Results

The performance of both the lightweight model and the normal-weight model were investigated with recycled brick masonry aggregate. Overall, building energy simulations were performed for the DOE reference model, lightweight C144 model, lightweight RBMA model, normal-weight C144 model, and normal-weight RBMA model. After the

reference strip mall model was validated against results provided by the DOE, the fully grouted lightweight and normal-weight concrete masonry with C144 mortar building envelopes were substituted for the basic steel-frame envelope.

Miami, FL, is classified as Zone 1A (hot-humid) by the IECC climate zone maps. Hot-humid is defined by the DOE as “a region that receives more than 20 inches (50 cm) of annual precipitation,” (U.S. DOE, 2010). Another required condition is that the temperature must be greater than 67°F (19.5°C) or higher for 3000 or more hours during the warmest six consecutive months of the year, or the temperature must remain above 73°F (23°C) for 1500 or more hours during the warmest six consecutive months of the year. Figures 2-4 show the annual percentage of energy consumption by category for the reference strip mall model, lightweight C144 concrete masonry model, and the normal-weight C144 concrete masonry model, respectively. Interior lighting was the largest consumer of energy for all three models. The only variances were in the heating (natural gas), cooling, and fan usage.

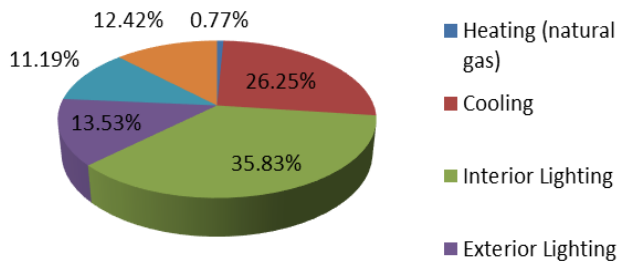


Figure 2. Miami, FL, Strip Mall DOE Reference Model Annual Energy Consumption by End-Use

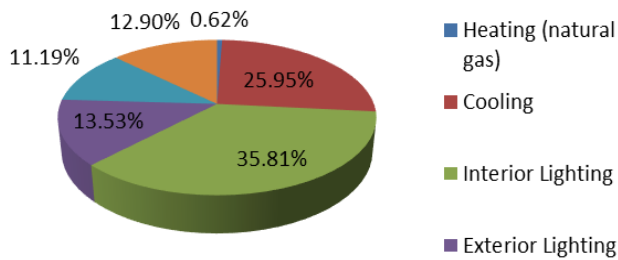


Figure 3. Miami, FL, Strip Mall Lightweight C144 Concrete Masonry Model Annual Energy Consumption by End-Use

Figures 5 and 6 show the end-use energy consumption for lightweight RBMA and normal-weight RBMA mortar models. As with the baseline models for Miami, the main source of end-use energy consumption was the interior lighting. Slight variations in heating (natural gas), cooling, and fan usage can be observed.

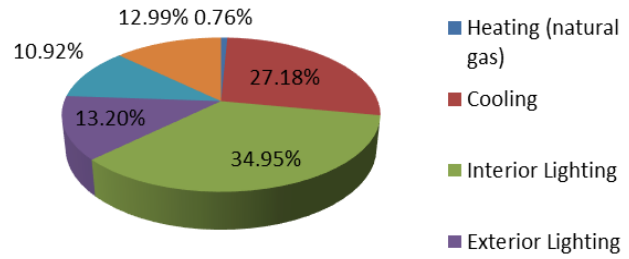


Figure 4. Miami, FL, Strip Mall Normal-Weight C144 Concrete Masonry Model Annual Energy Consumption by End-Use

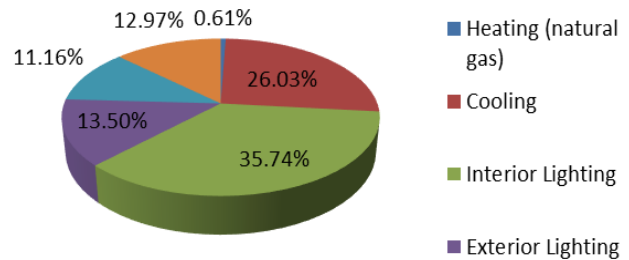


Figure 5. Miami, FL, Strip Mall Lightweight Concrete Masonry Model with RBMA Mortar Annual Energy Consumption by End-Use

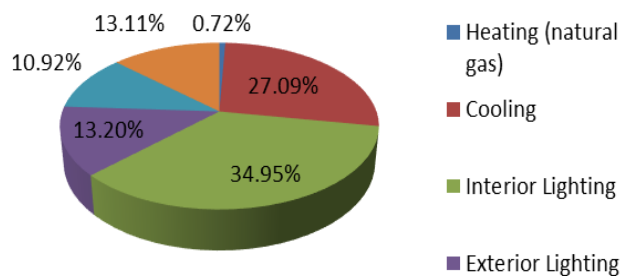


Figure 6. Miami, FL, Strip Mall Normal-Weight Concrete Masonry Model with RBMA Mortar Annual Energy Consumption by End-Use

An energy efficiency decrease of 0.04% for the lightweight C144 model was the most notable change in percent difference between the three lightweight models and the DOE reference model. The energy usage for the lightweight C144 model had an energy efficiency increase of 19.83% for heating (natural gas), an increase of 1.10% for cooling, and a 3.90% decrease for fans. Despite the large increase in heating efficiency, the total efficiency did not increase very much. This was due to the heating only accounting for a total of 0.62% of the entire end-use energy consumption. The lightweight RBMA models decreased in energy efficiency by 0.26% and 0.19%, respectively. Normal-weight

models varied little from one another in the total amount of energy consumption. The normal-weight C144 and RBMA models both decreased 2.50% in energy efficiency. Overall, heating (natural gas) increased 4.96%, cooling decreased 5.71%, and fan usage decreased 8.14% in energy efficiency, compared to the DOE reference model. Any of the lightweight models would be a suitable replacement for the DOE steel-frame reference model; however, the best performance was the lightweight C144 model.

An hourly heating and cooling analysis was performed in EnergyPlus for heating and cooling usage over peak temperature weeks for winter and summer. The heating and cooling hourly analyses were performed separately for a comparison of the lightweight models to the DOE reference model results, and the normal-weight models to the DOE reference model results. Hourly data were then combined to report total energy use for the two critical weeks. Due to the hot-humid climate in Miami, heat was only used for a few hours during the coldest week of the year. The use of heat between the lightweight C144 model and the lightweight recycled aggregate mortar models remained consistent with the number of hours the heat operated. The heat operated for a total of fifteen hours from January 1st to January 8th for the lightweight models. Even though the lightweight models operated the same number of hours, the DOE reference model consumed a total of 2.065 GJ, which was higher than any of the lightweight models. The lightweight C144 and lightweight RBMA models consumed 2.013 GJ and 2.021 GJ. A 2.52% increase in energy efficiency was experienced between the lightweight C144 model and the DOE reference model. The RBMA lightweight model experienced an increase in energy efficiency of 2.11%.

The normal-weight concrete masonry models performed differently than the lightweight concrete masonry models. The heat operated for a total of 21 hours over eight days, in contrast to the 15 hours over eight days for the DOE reference model and the lightweight models. This created a large difference in the amount of energy consumed through the peak winter week. All of the normal-weight model hourly consumption results were roughly around the same. For the normal-weight C144 model, 2.495 GJ were consumed and 2.431 GJ were consumed for the normal-weight RBMA model. These values are approximately 0.400 GJ greater than the DOE reference model. A 20.82% decrease in energy efficiency was seen from the DOE reference model to the normal-weight C144 model. Even though the normal-weight C144 model performed poorly, the normal-weight RBMA model performed slightly better. The energy efficiency decreased by 17.71% for the normal-weight RBMA model. Based on the analyses on heating energy consumption between the lightweight, normal-weight, and DOE reference models, the normal-weight models performed poor-

ly. The lightweight models consumed less energy than the DOE reference model.

Due to the hot-humid climate in Miami, cooling systems were running for the majority of the day during the warmest month of the year. The lightweight C144 model and the lightweight recycled aggregate mortar models remained consistent with the amount of energy used for cooling and the number of hours the cooling system was operating. The lightweight models consumed 10.637 GJ for the C144 model and 10.705 GJ for the RBMA model. Cooling energy consumption for the DOE reference model was only 10.560 GJ and operated for a total of 109 hours from January 1st through January 8th. Like the DOE reference model, the lightweight concrete masonry models' cooling systems also ran for a total of 109 hours over the same time period. In comparison to the DOE reference model, the lightweight C144 and lightweight RBMA models decreased in energy efficiency by 0.73%, 1.38%, and 1.17%, respectively. Of the two lightweight concrete masonry models, the C144 model performed the best. The normal-weight models consumed approximately 0.5 GJ more while cooling than the lightweight models. Half a gigajoule means that there is a larger energy gap between the DOE reference model and the normal-weight models. The normal-weight models consumed 11.384 GJ for the C144 model and 11.370 GJ for the RBMA model.

Even though the weekly sum of the cooling energy consumption was higher for the normal-weight models, the number of hours required to cool the facility remained at 109 hours. A 7.80% decrease in energy efficiency was seen from the DOE reference model to the normal-weight C144 model. The normal-weight expanded slate and RBMA models also decreased in energy consumption, but by slightly less at 7.67% and 7.60%. Both the lightweight models and the normal-weight models exceeded the energy usage of the DOE reference model for cooling. Although the energy consumption was greater, it only exceeded the DOE reference model by a very small amount. Miami experiences intense summer temperatures and requires a large amount of energy for cooling. The normal-weight models consumed more energy, but the normal-weight recycled aggregated variations outperformed the normal-weight C144 model. The DOE reference model or lightweight concrete masonry models would be a suitable energy efficient choice, based on these results.

An energy consumption analysis was performed for fan usage during the winter and summer. Fan energy consumption peak weeks are from January 1st to January 8th, and July 1st to July 8th. During the winter, fan energy consumption was much higher than the fan energy consumption during the summer. The percent difference in the fan energy con-

sumption during summer versus winter was consistently 3.60%. Interestingly, the fan energy consumption was consistent during the winter and summer peak weeks. Phoenix was classified by the IECC climate map as Zone 2B, hot-dry. Mix-humid climate conditions are defined as a region where the monthly outdoor temperature remains greater than 45°F (7°C) year round with less than 20 inches (50 cm) of annual precipitation (U.S. DOE 2011). These conditions are applicable to IECC zones 2 and 3.

Figures 7-9 show the percentages of annual energy consumption by end-use for the DOE reference, lightweight concrete masonry, and normal-weight concrete masonry simulations in Phoenix. Ranging from 31.88% (normal weight) to 33.97% (lightweight) energy consumption, lighting consumed the most energy. Cooling consumed the second highest amount of energy, ranging from 18.46% (lightweight) to 20.09% (normal weight). A hot-dry climate requires more cooling than other climate classifications.

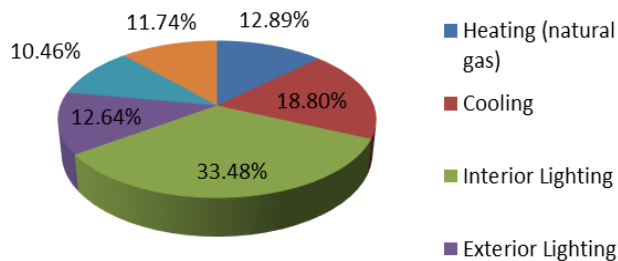


Figure 7. Phoenix, AZ, Strip Mall DOE Reference Model Annual Energy Consumption by End-Use

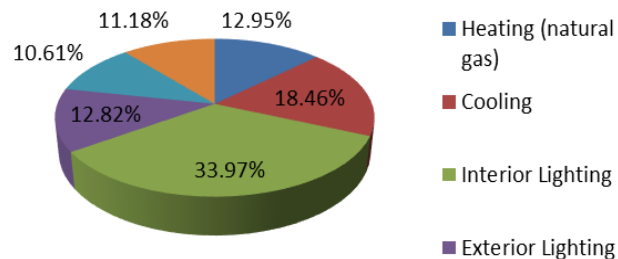


Figure 8. Phoenix, AZ, Strip Mall Lightweight C144 Concrete Masonry Model Annual Energy Consumption by End-Use

Figures 10 and 11 shows annual end-use energy for the lightweight RBMA and normal-weight RBMA mortar models. For the lightweight and normal-weight models, the main consumers of energy were interior lighting and cooling. More energy was required for cooling, due to the warmer climatic conditions in Phoenix. Interior lighting for the lightweight models consumed nearly a third of the overall annual energy consumption. The lightweight C144 model

consumed 33.97%, while the lightweight models consumed 33.87% and 33.93%, respectively. The second largest consumer of the annual end-use energy was cooling. Cooling increased from the lightweight C144 model to the lightweight recycled aggregate mortar models. The lightweight C144 model cooling consumption was equal to 18.46% and increased to 18.58% for the lightweight RBMA model. Like the cooling energy consumption, the fan energy consumption also increased from the lightweight C144 model to the lightweight recycled aggregate mortar models. Fans consumed 11.18% of the energy for the lightweight C144 model, and 11.26% was consumed for the lightweight RBMA model. Heating was the last main consumer of annual end-use energy for the lightweight models. Energy consumption for heating decreased from the lightweight C144 model to the lightweight recycled aggregate mortar models. The lightweight C144 model energy consumption was equal to 12.95%, and the recycled aggregate mortar models consumed 12.93% (RBMA) and 12.90% (expanded slate).

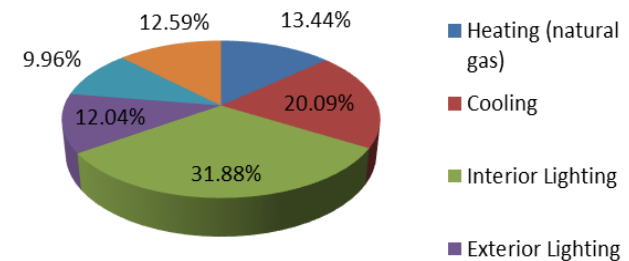


Figure 9. Phoenix, AZ, Strip Mall Normal-Weight C144 Concrete Masonry Model Annual Energy Consumption by End-Use

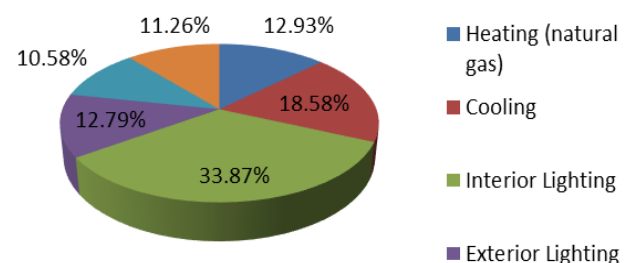


Figure 10. Phoenix, AZ, Strip Mall Lightweight Concrete Masonry Model with RBMA Mortar Annual Energy Consumption by End-Use

The Phoenix normal-weight models were similar to the lightweight models in that the interior lighting also consumed about a third of the annual end-use energy consumption. In contrast, the interior lighting consumption for the normal-weight models decreased from the C144 model to the recycled aggregate mortar models. The normal-weight

C144, RBMA, and expanded-slate models were equal at 31.88%, 32.04%, and 32.08%, respectively. The second largest consumer of end-use energy was cooling. Similar to the lightweight models, the normal-weight model cooling consumption decreased from the normal-weight C144 model to the recycled aggregate mortar models. The normal-weight C144 model consumed 20.09%, and 20.04% was consumed by the normal-weight RBMA model. Unlike the lightweight models, the next largest consumer of energy for the normal-weight models was heating. The energy consumption increased from 13.44% for the normal-weight C144 model to 13.38% (RBMA). The final main consumer of energy for the normal-weight Phoenix models was the fan usage. The fan usage percentage decreased from 12.59% for the C144 model to 12.44% for RBMA.

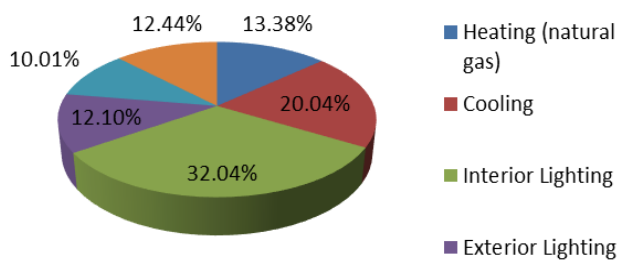


Figure 11. Phoenix, AZ, Strip Mall Normal-Weight Concrete Masonry Model with RBMA Mortar Annual Energy Consumption by End-Use

The lightweight concrete masonry model increased in energy end-use efficiency for heating, cooling, and fan usage. Heating increased by 0.94%, cooling increased by 3.23%, and fan usage increased by 6.14%, for a total increase in energy end-use efficiency of 1.45%. The lightweight RBMA model increased energy consumption efficiency by 1.15%. Any of these options would be an energy efficient replacement in Phoenix for the DOE steel-frame reference model. Unlike the lightweight models, the normal-weight models increased in energy consumption for all models. The normal-weight C144 model decreased by 4.99% and the normal-weight RBMA model decreased by 4.49% in energy efficiency. According to the data the lightweight concrete masonry building envelope responded to high-heat climate conditions better than the normal-weight concrete masonry and steel-frame reference models. Due to the reduction in energy consumption, any of the lightweight concrete masonry options would be ideal.

Hourly heating and cooling energy consumption over peak temperature weeks for winter and summer were analyzed for the EnergyPlus model results. Results of the models were analyzed by separating them into lightweight model results and normal-weight model results, then comparing

them to the DOE reference model results for winter and summer. The heating energy consumption difference between the lightweight model and lightweight recycled aggregate mortar models and the DOE reference model was no greater than 1.10 GJ. The lightweight RBMA model operated for a total of 97 hours over eight days. The lightweight C144 model number of heating operating hours deviated only slightly from the other model with 95 hours. The DOE reference model only consumed a total of 12.934 GJ over 75 hours for the entire peak week in January, whereas the lightweight C144 and RBMA models consumed a total of 12.832 GJ and 13943 GJ. Only a slight decrease in energy efficiency occurred. The lightweight C144 model and RBMA model experienced decreases of 6.95% and 7.80% in energy efficiency, respectively. The lightweight C144 model performed the best. The moderate heating energy usage was due to the less extreme winter temperatures experienced in Phoenix. The normal-weight C144 model and normal-weight recycled aggregate mortar models experienced a similar amount of hours for heating operation. Hours of heating operation for the normal-weight models were 94 (C144) and 97 (RBMA).

Even though the normal-weight C144 model operated heat the fewest number of hours for the normal-weight models, it consumed the largest amount of energy at 15.399 GJ. Energy consumption for the remaining model was 15.383 GJ for the normal-weight RBMA model. The normal-weight models deviated from the C144 model about 2.4 GJ. Unlike the lightweight models, the normal-weight models experienced a large decrease in energy efficiency. The normal-weight C144 model decreased 19.06% and the normal-weight RBMA model decreased 18.94%. Of the two normal-weight models, the RBMA model performed the best. Overall, the lightweight concrete masonry models did not stray far from each other for the amount of heating energy consumed. This trend was also true for the normal-weight concrete masonry models. The DOE reference model remained the best option for a more energy efficient building, due to the increased energy consumption for heating during the peak winter temperatures in Phoenix.

From July 1st to July 8th, cooling consumption data were recorded every hour for the lightweight concrete masonry models and the DOE reference model. The cooling system ran for a moderate amount of the day, due to the mixed-humid climate and hot summer weather. The lightweight concrete masonry models consumed more energy over the first week of July than the DOE reference model. Even though the DOE reference model consumed more energy during peak hours, the weekly total energy consumption was 11.004 GJ, which was less than all of the lightweight models. Cooling energy consumption numbers for the lightweight models were 11.024 GJ for the C144 model and

11.152 GJ for the RBMA model. All of the lightweight models required 109 hours to cool the facility, which was four hours more per week than the DOE reference model.

The increase in cooling energy consumption for the lightweight models correlated with the increase in the amount of hours required to cool the facility. There was a slight decrease in energy efficiency for the lightweight models. The C144 model decreased 0.18% and the RBMA model decreased 1.34. Overall, the lightweight C144 model performed the best. Like the lightweight concrete masonry models, the normal-weight models consumed more energy cooling the strip mall in Phoenix than the DOE reference model. The normal-weight models consumed 12.785 GJ over 112 hours for the C144 model and 12.727 GJ over 111 hours for the RBMA model. The DOE reference model only consumed 11.004 GJ over 105 hours. The normal-weight models were considerably less energy efficient than the lightweight models. The normal-weight C144 and RBMA models decreased in energy efficiency by 16.19% and 15.66%, respectively. The lightweight and normal-weight models both consume more energy than the DOE reference model while cooling the strip mall. Of the alternative building envelope constructions, the lightweight models were the closest in cooling energy consumption to the DOE reference model. In conclusion, the DOE reference model outperformed the lightweight and normal-weight models and was also the most energy efficient option.

Conclusions

The U.S. Department of Energy (DOE) reported in 2012 that the building industry was the largest consumer of natural resources and electricity. In order to address the impact of the construction industry on the environment, the use of raw, virgin aggregate and energy efficiency must improve. Commercial building energy consumption is currently being addressed by the building sector by investigating new materials, building envelopes, and energy efficiency best practices. Growth in the new construction sector places a higher demand on natural aggregate, resulting in an escalation in natural aggregate costs. The focus of this current study was to determine the impact on specific heat capacity and thermal conductivity using recycled demolition waste aggregates in masonry mortar and grout applications. A possible solution for reducing demand on natural aggregates is the use of expanded slate and recycled brick aggregate in masonry mortar applications.

In this study, the thermal properties of the recycled aggregate mortar were obtained from previous studies in order to create a comparative analysis between the DOE strip mall steel-frame model, normal-weight and lightweight concrete

masonry models, and normal-weight and lightweight recycled aggregate models in the EnergyPlus BESP. The objectives achieved by this study were:

- A model using building energy simulation programs (BESP) for a concrete masonry structure using recycled aggregates was developed and validated by creating a model in EnergyPlus and comparing the results to the DOE results.
- Models for each masonry mortar aggregate were successfully developed and simulated.
- A comparative analysis of annual energy consumption by end-use, the annual building utility performance summary, the heating, cooling, and fan energy usage for peak winter and summer weeks, and the total annual cost and utility usage were performed. Results indicated that the recycled aggregate mortar models performed as well or better than the lightweight and normal-weight masonry systems.

The model results showed that in Miami, FL, the concrete masonry models did not perform as well as the DOE reference model; however, the recycled aggregate mortar models performed as well as and sometimes better than the lightweight and normal-weight concrete masonry models. During the peak summer week, the normal-weight expanded slate and normal-weight C144 models decreased in energy efficiency by 7.60% and 7.80%, respectively. A similar outcome was observed for the peak winter week also. The normal-weight expanded slate and normal-weight C144 models decreased in energy efficiency by 17.45% and 20.82%, respectively. The lightweight C144 model proved to be most energy efficient for both heating and cooling. The lightweight expanded slate model actually increased in energy efficiency by 2.89% while heating.

A percent decrease was experienced in Phoenix, AZ, for both cooling and heating energy efficiency. The most energy efficient models for cooling energy efficiency were the lightweight C144 and normal-weight expanded slate models. These models experienced decreases of 0.18% and 15.36% in energy efficiency, respectively. The heating energy consumption performed similarly except that the decrease in energy efficiency was greater. The lightweight C144 model and the normal-weight expanded slate models performed the best, with decreases of 6.95% and 18.83% energy efficiency, respectively. Although there was a decrease in energy efficiency for all of the models, the recycled aggregate mortar models performed as well as or better than the C144 concrete masonry models. The energy use model results showed that the RBMA models consistently performed as well as, if not better than, the lightweight and normal-weight C144 models. By replacing sand with RBMA in mortar mixes, a more environmentally conscious

material can be created. Recycled aggregate mortar will help to reduce demolition waste aggregates, maintain competitive aggregate costs, decrease the need for new quarrying sites, and contribute to a more sustainable building envelope design.

References

- [1] Gilpin, R. R., Hyun, H., & Menzie, D. W. (2004). Recycling of construction debris as aggregate in the Mid-Atlantic Region, USA. *Resources, Conservation, and Recycling*, 42(3), 275-294.
- [2] Sonawane, T. R., & Pimplikar, S. S. (2013). Use of recycled aggregate in concrete. *International Journal of Engineering Resource Technology*, 2(1), 1-9.
- [3] Oikonomou, N. D. (2005). Recycled concrete aggregates. *Cement and Concrete Composites*, 27, 315-318.
- [4] Environmental Protection Agency. (2012). Construction and Demolition (C&D) Debris. Retrieved from <http://www.epa.gov/reg3wcmd/solidwastecd.html>
- [5] Jha, K. N., Misra, S., & Rao, A. (March 2007). Use of aggregates from recycled construction and demolition waste in concrete. *Resources, Conservation, and Recycling*, 50(1), 71-81.
- [6] Hansen, T. C. (1992). *Recycling of Demolished Concrete and Masonry*. Taylor and Francis, Oxfordshire, UK.
- [7] Etxeberria, M., Marí, A. R., & Vázquez, E. (2007). Recycled aggregate concrete as structural material. *Materials and Structures*, 40(5), 529-541.
- [8] Khalaf, F.M., & DeVenny, A. S. (2004). Recycling of demolished masonry rubble as coarse aggregate in concrete: review. *Journal of Materials in Civil Engineering*, 16(4), 331-340.
- [9] Behera, M., Bhattacharyya, S. K., Minocha, A. K., Deoliya, R., & Maiti, S. (2014). Recycled aggregate from C&D waste & its use in concrete—a breakthrough towards sustainability in construction sector: A review. *Construction and Building Materials*, 68, 501-516.
- [10] Tempest, B., Cavalline, T., Gergely, J., & Weggel, D. (2010). Construction and Demolition Waste Used as Recycled Aggregates in Concrete: Solutions for Increasing the Marketability of Recycled Aggregates Concrete. *Proceedings of the Concrete Sustainability Conference sponsored by the National Ready Mixed Concrete Association (NRMCA)*, (pp.1-44). Tempe, AZ.
- [11] Gonzalez, G. P., & Moo-Young, H. K. (2004). *Transportation Applications of Recycled Concrete Aggregate*. FHWA State of the Practice National Review. Federal Highway Administration.
- [12] Saeed, A. (2008). *Performance-Related Tests of Recycled Aggregates for Use in Unbound Pavement Layers*. National Cooperative Highway Research Program, Report 598.
- [13] Corinaldesi, V., & Moriconi, G. (2009). Influence of mineral additions on the performance of 100% recycled aggregate concrete. *Construction and Building Materials*, 23, 2869-2876.
- [14] Juan, M. S., & Gutierrez, P. A. (2009). Study on the influence of attached mortar content on the properties of recycled aggregate concrete. *Construction and Building Materials*, 23, 872-877.
- [15] Butler, L., West, J. S., & Tighe, S. L. (2011). The effect of recycled concrete aggregate properties on the bond strength between RCA concrete and steel reinforcement. *Cement and Concrete Research*, 41 (10), 1037-1049.
- [16] Kwan, W. H., Ramli, M., Kam, K. J., & Sulieman, M. Z. (2012). Influence of the amount of recycled coarse aggregate in concrete design and durability properties. *Construction and Building Materials*, 26, 565-573.
- [17] Butler, L., West, J. S., & Tighe, S. L. (2013). Effect of recycled concrete coarse aggregate from multiple sources on the hardened properties of concrete with equivalent compressive strength. *Construction and Building Materials*, 47, 1292-1301.
- [18] Debeib, F., & Kenai, S. (2008). The use of coarse and fine crushed bricks as aggregate in concrete. *Construction and Building Materials*, 22(5), 886-893.
- [19] Yang, J., Du, Q., & Bao, Y. (2011). Concrete with recycled concrete aggregate and crushed clay bricks. *Construction and Building Materials*, 25, 1935-1945.
- [20] Cavalline, T., & Weggel, D. (2013). Recycled Brick Masonry Aggregate Concrete: Use of Brick Masonry from Construction and Demolition Waste as Recycled Aggregate in Concrete. *Structural Survey*, 31(3), 160-180.
- [21] Nicholas, T., Radford, P., Cavalline, T., & Brizendine, A. L. (2014). Compressive Performance of Recycled Aggregate Mortar. *The International Journal of Engineering Research and Innovation*, 6 (2), 49-55.
- [22] Graber, D. W., Lang, N. R., Mariscal, G., Thompson, J. J., & Witthuhn, T. (2012). Thermal Catalog of Concrete Masonry Assemblies. *National Concrete Masonry Association*, 2, 6-9.
- [23] Ledesma, E. F., Jiménez, J. R., Fernández, J. M., Galvín, A. P., Agrela, F., & Barbudo, A. (2014). Properties of masonry mortars manufactured with fine recycled concrete aggregates. *Construction and Building Materials*, 71, 289-298.

-
- [24] Martínez, I., Etxeberria, M., Pavón, E., & Díaz, N. (2013). A comparative analysis of the properties of recycled and natural aggregate in masonry mortars. *Construction and Building Materials*, 49, 384-392.
- [25] ACI Committee 122. (2014). *Guide to Thermal Properties of Concrete and Masonry Systems*. ACI 122R-14. Farmington Hills, MI: American Concrete Institute.
- [26] Tatro, S. B. (2006). *Thermal Properties. Significance of Tests and Properties of concrete and Concrete-Making Materials*, (pp. 226-237). STP 169D, ASTM International, West Conshohocken, PA.
- [27] U.S. Department of Energy (30 April 2013). About Energy Plus. Retrieved from http://apps1.eere.energy.gov/buildings/energyplus/energyplus_about.cfm.
- [28] National Renewable Energy Laboratory. OpenStudio. (2013). Retrieved from <http://openstudio.nrel.gov>
- [29] National Renewable Energy Laboratory (2011). *U.S. Department of Energy Commercial Reference Building Models of the National Building Stock*. National Renewable Energy Laboratory, NREL/TP-550-46861.
- [30] Crawley, D. B., Lawrie, L. K., Pedersen, C. O., & Winkelmann, F. C. (2000). EnergyPlus: Energy Simulation Program. *American Society of Heating, Refrigerating, and Air-Conditioning Engineers*, 42(4), 49-56.

MORGAN LANEY holds BS and MS degrees in Civil Engineering Technology and Construction Management from UNC Charlotte. Mr. Laney may be reached at mlaney@uncc.edu

Biographies

THOMAS NICHOLAS II, PhD, PE, is the Undergraduate Program Coordinator and Assistant Professor of Civil Engineering Technology and Construction Management at UNC Charlotte. Dr. Nicholas holds graduate degrees from West Virginia University (MSCE) and UNC Charlotte (PhD), and is a registered professional engineer in North Carolina. Dr. Nicholas may be reached at tmichola@uncc.edu

TARA L. CAVALLINE, PhD, PE, is an assistant professor of Civil Engineering Technology at UNC Charlotte. She holds BS and MS degrees in Civil Engineering from the Pennsylvania State University and a PhD in Infrastructure and Environmental Systems from UNC Charlotte and is a registered professional engineer in North Carolina. Dr. Cavalline may be reached at Tara.Cavalline@uncc.edu

DIXIE JOHNSON is an undergraduate research assistant in Civil Engineering Technology and Construction Management at UNC Charlotte. Ms. Johnson may be reached at djohn223@uncc.edu

CONCRETE WITH ENHANCED DUCTILITY USING STRUCTURAL MICROFIBERS

Shane M. Palmquist, Western Kentucky University; Ramyasree Annam, Western Kentucky University

Abstract

Concrete, one of the most widely used construction materials in the world, is typically composed of portland cement; water; aggregates such as sand, gravel, or crushed stone; and admixtures. Unlike steel, concrete is a quasi-brittle material. For design purposes, the tensile strength of concrete is negligible, since it is relatively weak in tension. Reinforcing steel is added to concrete for this purpose because steel is relatively strong in tension and has greater ductility. In recent years, materials like fiber-reinforced cementitious composites have been explored and developed. Many types of fibers with varying sizes have been examined in concrete in hopes of developing more ductile cementitious materials than traditional concrete. The components of these fiber-reinforced cementitious materials are similar to traditional concrete, except no coarse aggregates are used and air entrainment is not necessary. And, like traditional concrete, fiber-reinforced cementitious materials are cost effective. Numerous large-scale potential applications exist, including buildings, bridges, airports, culverts, dams, and projects involving repair or rehabilitation work.

In this paper, the authors present the results of a fiber-reinforced cementitious composite that has been developed over time, and based on work reported in the literature with modifications based on experimentation of mix designs using high-performance polyvinyl acetate (PVA) microfibers. Cube test specimens were cast and tested in compression and indirect tension. In addition, a large-chamber scanning electron microscope examined fiber crack bridging of post-failed cube specimens that were loaded in indirect tension (split cube tests). Results showed that test specimens of concrete reinforced with PVA microfibers exhibited a decrease in compressive strength, but a significant increase in indirect tensile strength, and have more ductility than specimens not containing the fibers, such as more traditional types of concrete.

Introduction

In the last few decades, growing interest has developed in using fibers in ready-mixed concrete, precast concrete, and shotcrete. Fibers made from steel, plastic, glass, wood, and other materials have been used in concrete. Fibers are typically added to concrete mixes in low-volume dosages, often

at rates less than 1.0%, for purposes of reducing plastic shrinkage cracking [1]. However, fibers do not affect the free shrinkage of concrete, but, given high enough dosages, fibers can increase resistance to cracking as well as decrease the size of the crack widths [2]. Generally, fiber-reinforced concrete is grouped into two classes: thin-sheet products and bulk structure products. Fiber fraction volumes further determine subclassifications and uses for each class, with low-volume fiber fractions (<1%) primarily serving to resist plastic shrinkage and high-volume fiber fractions (2>-10%) serving to provide additional or secondary reinforcement to main reinforcing steel. High volumes (up to 20% steel fibers) have been demonstrated to significantly improve all strength properties. Fiber-reinforced concrete has become synonymous with various steel fiber reinforcements. However, the addition of steel fibers increases weight. Perhaps concrete in the form of a cementitious composite could be developed that utilizes nonferrous structural fibers. This material would capitalize on the additional strength of fibers, while providing a significantly lighter composite material. One such possibility is the use of synthetic polymer fibers.

Synthetic fibers are the result of research and development in the petrochemical and textile industries. Synthetic fibers that have been used in portland cement concrete include acrylic, aramid, carbon, nylon, polyester, polyethylene, and polypropylene. One problem with synthetic fibers is their ability to disperse and distribute evenly in the composite, providing a compatible and continuous bond between the fibers and the cementitious paste matrix. Polypropylene fibers are commonly used as a fiber in portland cement concrete, since the fibers are chemically inert, hydrophobic, and lightweight. Fibers of this type are generally added at a rate of 0.1% by volume of concrete. Polypropylene fibers can reduce plastic shrinkage cracking and help reduce concrete spalling.

Figure 1 shows how, for many years, researchers have attempted to produce concrete that is more ductile in behavior [3, 4]. In most cases, ductile concrete has been achieved using fiber reinforcement. Concrete with synthetic polymer fibers, such as polypropylene microfibers, was the result of this development effort. This material has demonstrated impressive ductile behavior. Bending can be achieved with a high level of inelastic deformation resulting from the development of numerous microcracks with limited crack

widths. This is in sharp contrast to traditional concrete, where a single point of failure (crack with a large crack width) develops from excessive bending. Research and development by Li [5, 6] has produced a cementitious material using these types of fibers, which has greater ductility than traditional types of concrete. This material has been used in a number of projects worldwide and was proposed for many others [7]. The largest use of this material to date has been as a 5-mm thick topcoat on the Mihara Bridge in Hokkaido, Japan. Domestically, the Michigan Department of Transportation has used this material for surface repair projects and as a flex joint for replacement of a steel expansion joint on a bridge deck crossing over I-94 in Ypsilanti, Michigan.

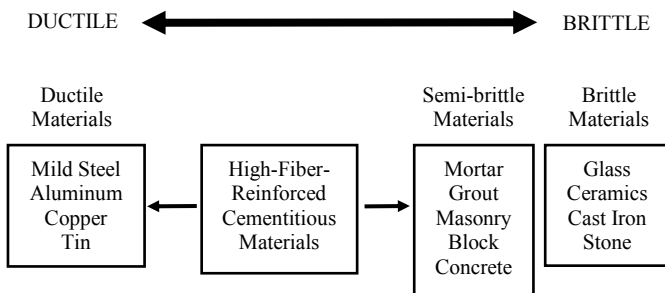


Figure 1. Range of Ductile-to-Brittle Behavior of Materials

In this current study, the authors examined a type of concrete reinforced with PVA microfibers and compared it with the same concrete without fibers. The project was conducted in two phases: first to cast cubes in order to compare compressive and indirect tensile strengths of the concrete with and without PVA microfibers, and then to use a large-chamber, scanning electron microscope to examine PVA microfiber bridging across concrete cracks of cube specimens that were loaded to failure in indirect tension (split cube tests).

Polyvinyl Alcohol Microfibers

Polyvinyl alcohol (PVA) microfibers at the molecular level consist of repeated structural units of $[-CH_2-CH(OH)-]_n-$. Using PVA microfibers as a reinforcement material leads to many benefits. Apart from being economical, the PVA microfiber reinforcement improves the quality of concrete by making it fatigue and corrosion resistant. Polyvinyl acetate is the starting material in the manufacturing of polyvinyl alcohol (PVA). PVA is hydrolyzed by treating it with an alcoholic solution in the presence of an aqueous acid or alkali. OH groups present in PVA can form hydrogen bonds between the fibers and the cement matrix. The resulting surface bonding helps in bridging across cracks. Figure 2 shows that the tensile strength of PVA fibers is significantly higher than mild steel rebar used in reinforced concrete,

which also contributes to improved bridging performance when cracks develop and propagate.



Figure 2. KURALON Ultra-High-Performance Nycon PVA Microfibers

Comparative Concrete Batch Designs

Figure 3 shows the two batches of concrete that were cast: the first was the baseline concrete containing no microfibers, and the second was reinforced with 8-mm PVA microfibers added at a volume fraction of 2.2%. All other components were measured and kept identical to the baseline concrete for comparative purposes. Portland cement type III was used since it is finer than type I. Super plasticizer Glenium 3000 NS, a high-range water reducing admixture, was used to increase the workability of concrete. The resulting mix was prepared using a water-to-cement ratio of 0.59. Table 1 summarizes the mix design used to establish the baseline concrete cube tests, where the amount of each component is given in kilograms per cubic meter of concrete cast.

Table 1. Concrete Mix Proportions

Component	Amount (kg/m ³)
Portland cement (type III)	605.5
Fine aggregate (sand)	484.4
Fly ash (type C)	726.6
Water	353.2
Super plasticizer (Glenium 3000 NS)	8.6



Figure 3. Incorporation of PVA Microfibers in Concrete

Experimental Tests

All other mix proportions were the same between the two concrete batches. Each batch produced a total of 48 specimens, which were 50x50x50 mm cubes. From each batch, 24 cubes were tested in compression, while the other 24 cubes were tested in indirect tension (split cube test). For the baseline concrete, four cubes each were tested in compression at 1, 3, 7, 14, 21, and 28 days to determine the compressive strength gain as a function of curing time. The same was performed for the concrete reinforced with PVA microfibers. Also for the baseline concrete, four cubes each were tested in indirect tension (split cube test) at 1, 3, 7, 14, 21, and 28 days to determine the indirect tensile strength gain as a function of curing time. Figure 4 shows how this was also done for the concrete reinforced with PVA microfibers. Indirect tensile strength (split cube tensile strength) was calculated using Equation (1):

$$\sigma_{sp} = 0.519 P / S^2 \quad (1)$$

where, P is the failure load in Newtons and S is the length of the side in millimeters of the concrete cube [8].

A large-chamber, scanning electron microscope (LC-SEM) was used for imaging the cubes with fibers. These cubes were first tested in indirect tension (split cube test) and then examined using the LC-SEM. A vertical crack formed during the test, and the PVA microfibers were observed to be bridging across the cracks. To better demonstrate this bridging, imaging was done using an LC-SEM. LC-SEM is a scanning electron microscope, with a magnification power of up to 300,000x, used for high-resolution imaging. This instrument accommodates large samples without the need to cut them into small pieces, which damages the specimens. The images generated have a resolu-

tion greater than 10 nm. This instrument helped to better understand the nature of fiber bridging that occurred across the concrete cracks that developed. Figure 5 shows the LC-SEM available at the WKU NOVA Center, one of only two in the world.

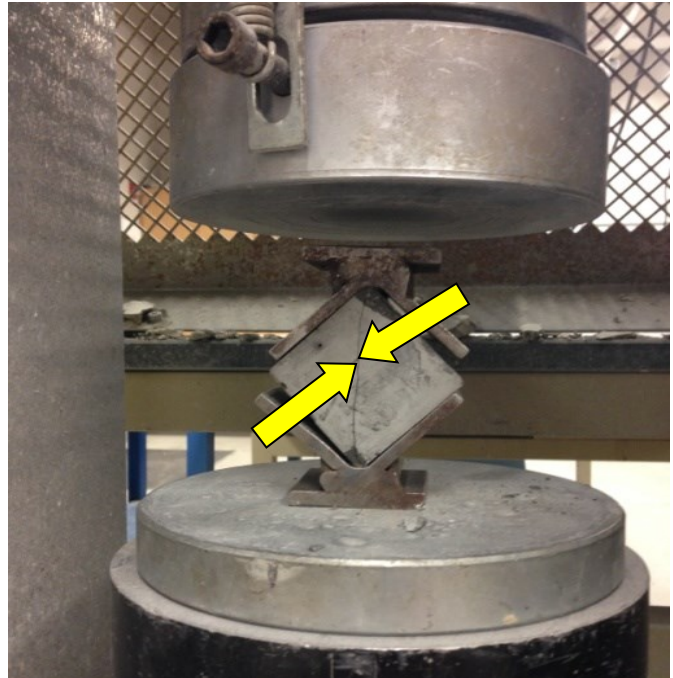


Figure 4. Vertical Crack in Split Tensile Strength Test Cube



Figure 5. Large-Chamber Scanning Electron Microscope at WKU NOVA Center

Test Results

Figure 6 shows the average compressive strength and the age of the concrete cubes with and without fibers. The concrete batch without fibers is referred to as the baseline concrete, while the other batch is referred to as the concrete with PVA fibers. Not including day 1 results, the fiber-reinforced concrete cubes exhibited an average of 26.7% less compressive strength than the cubes without fibers. The fibers in the composite cause the formation of voids in the presence of filling material (sand). This results in the improper packing of the concrete, thereby decreasing the compressive strength of the test specimen [9].

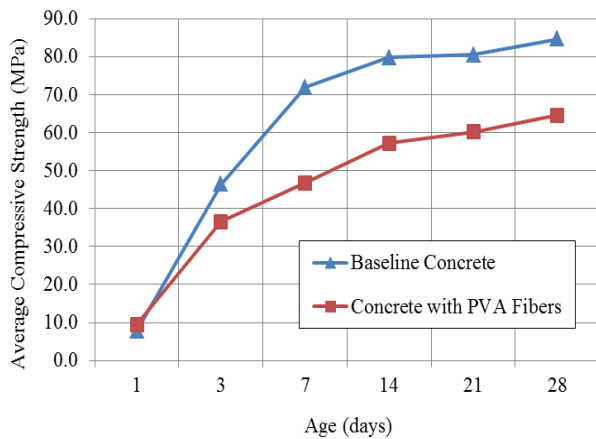


Figure 6. Compressive Strength at Various Ages

Figure 7 shows the average indirect tensile strength (split cube tensile strength) and the age of the concrete cubes with and without fibers. The fiber-reinforced concrete cubes exhibited an average of 57.4% more indirect tensile strength than the cubes without fibers.

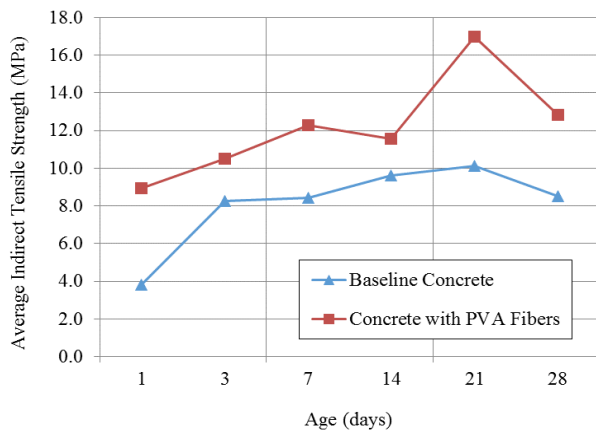


Figure 7. Indirect Tensile Strength at Various Ages

SEM images of concrete cubes tested for split tensile strength were collected. Figure 8 shows the fibers bridging across the crack. It also shows that the fibers are pulled between the crack and that they are under stress. When a crack is formed in PVA fiber-reinforced concrete, the fibers act as bridges or stitching between the cracks, which helps to prevent or limit the formation of macrocracks. These fibers undergo tension as they are pulled in between the cracks. PVA microfiber pullout from the cementitious matrix was not observed.

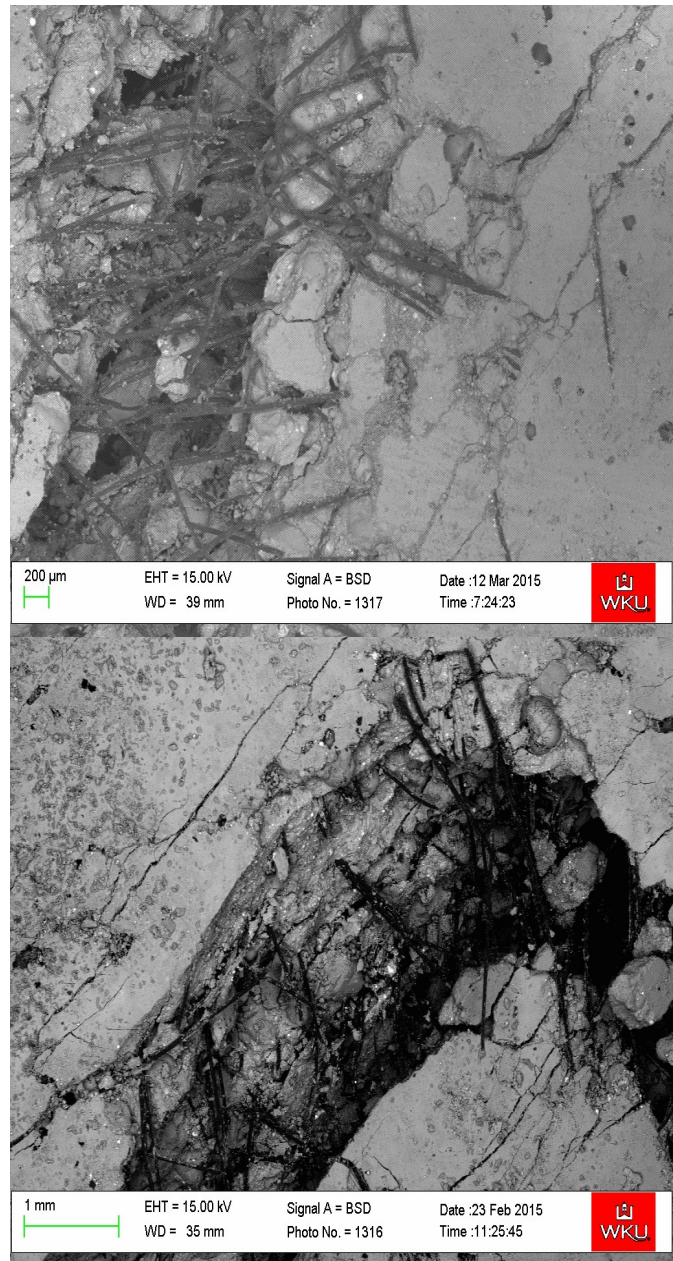


Figure 8. SEM Images of Fibers Bridging Cracks in the Concrete

Summary and Conclusion

In this study, the authors examined the effect of PVA fiber loading of 2.2% by volume on the mechanical properties of concrete. Compressive strength and indirect tensile strength testing was done for both baseline and PVA microfiber-reinforced concrete cubes. When compressive strength was examined as a function of curing time, the concrete cubes with PVA microfiber reinforcement exhibited 26.7% less compressive strength than the baseline concrete cubes, whereas when indirect tensile strength was examined as a function of curing time, the concrete cubes with PVA microfiber reinforcement exhibited 57.4% more indirect tensile strength than the baseline concrete cubes. An increase in the indirect tensile strength shows that the concrete has gained ductility. SEM imaging of the samples was done to observe fiber bridging across the concrete cracks. Based on the images collected, all cracks observed were shown to have PVA microfibers bridging across the crack widths. PVA microfiber pullout from the cementitious matrix was not observed.

Acknowledgements

The authors would like to thank the Foundation at Western Kentucky University for financial support of this project. The authors would also like to thank Dr. Cate Webb, associate dean of Ogden College at Western Kentucky University, for her support throughout this project as well as Dalton Hankins and Kyle Parks, two civil engineering seniors, for assisting in fabricating and testing the cubes in the materials laboratory. Finally, the authors are grateful to Dr. Edward Kintzel for assistance with the large-chamber, scanning electron microscope.

References

- [1] Kosmatka, S. H., Kerkhoff, B., & Panarese, W. C. (2006). *Design and control of concrete mixtures*. (14th ed.). Skokie, IL: Portland Cement Association.
- [2] Shah, S. P., Weiss, W. J., & Yang, W. (1998). Shrinkage cracking – Can it be prevented? *Concrete International*, 20(4), 51-55.
- [3] Li, V. (1997). *Engineered cementitious composites (ECC) – Tailored composites through micromechanical modeling*. Retrieved from https://deepblue.lib.umich.edu/bitstream/handle/2027.42/84667/csce_tailoredecc_98.pdf?sequence=1
- [4] Wang, S., & Li, V. (2005). *Polyvinyl alcohol fiber reinforced engineered cementitious composites: Material design and performances*. Retrieved from

- <http://citeseerx.ist.psu.edu/viewdoc/download?doi=10.1.1.67.4523&rep=rep1&type=pdf>
- [5] Li, V. C. (2003). On engineered cementitious composites (ECC) – A review of the material and its applications. *Journal of Advanced Concrete Technology*, 1(3), 215-230.
- [6] ASTM. (2004). *Annual book of standards, concrete and aggregates*. (Vol. 4.02). Philadelphia, PA: ASTM.
- [7] ECC Technology Network. (n.d.). Retrieved from http://www.engineeredcomposites.com/Applications/mihara_bridge.html
- [8] Badagha, G. D., & Modhera, D. C. (2013). Studies on harden properties of mortar using carbon fibers. *International Journal of Advancements in Research and Technology*, 2(3), 249-252.
- [9] Nuruddin, F. M., Khan, U. S., Shafiq, N., & Ayub, T. (2014) Strength development of high-strength ductile concrete incorporating metakaolin and PVA fibers. *The Scientific World Journal*, 1, 387259. doi: 10.1155/2014/387259

Biographies

SHANE M. PALMQUIST is an associate professor of structural engineering in the Department of Engineering at Western Kentucky University and is the Ritter Professor of Civil Engineering. Dr. Palmquist is also the coordinator of the civil engineering program and is a licensed professional engineer in Kentucky. Prior to becoming a faculty member at WKU, Dr. Palmquist was a bridge engineer for Lichtenstein Consulting Engineers in Natick, Massachusetts. He earned his BS degree in civil engineering from the University of New Hampshire in 1995; his MS in structural engineering from the University of Rhode Island in 1996; and his PhD in structures/materials engineering from Tufts University in 2003. His research and technical interests include project-based engineering education, cable-supported structures, and cementitious materials with enhanced properties using fibers. Dr. Palmquist may be reached at shane.palmquist@wku.edu

RAMYASREE ANNAM just completed her master of science degree from the Department of Chemistry at Western Kentucky University. Her thesis research focused on studying the mechanical properties of PVA fiber-reinforced concrete with Raman spectroscopy analysis. Ms. Annam may be reached at ramyasree.annam340@topper.wku.edu

INSTRUCTIONS FOR AUTHORS: MANUSCRIPT SUBMISSION REQUIREMENTS


The INTERNATIONAL JOURNAL OF ENGINEERING RESEARCH AND INNOVATION is an online/print publication. Articles appearing in IJERI generally focus on engineering-related research but also may branch out to diverse fields related to technological innovation and entrepreneurship. All submissions to this journal, including manuscripts, peer-reviews of submitted documents, requests for editing changes, as well as notification of acceptance or rejection, will be handled electronically.

All manuscript submissions must be prepared in Microsoft Word (.doc or .docx) and contain all figures, images, and/or pictures embedded where you want them and appropriately captioned. It is highly recommended that you print, in color, all images in your manuscript in order to determine their quality; the journal editors will be doing the same during the editorial review of your manuscript. If your manuscript is accepted for publication, you will receive instructions regarding all required revisions and the submission of higher-quality images. If you are able to provide such images, it's possible that you will be asked to remove them from the manuscript.

Tables must be created directly in Word, not imported as pictures, and be enclosed on all sides. If you have graphs or charts, they should also be created directly in Word, if possible. If that is not possible, the editor will discuss further options with you. Please be conscientious of the quality of your images and remember that all online and print copies of issues of IJERI are in color.

The editorial staff of the International Journal of Engineering Research and Innovation reserves the right to format and edit any submitted document in order to meet publication standards of the journal. Included here is a summary of the formatting instructions. You should, however, review the "[sample Word document](#)" included on our website (<http://ijeri.org/formatting-guidelines>) for a detailed analysis of how to correctly format your manuscript.

The references included in the References section of your manuscript must follow APA-formatting guidelines. In order to help you, the sample Word document also includes numerous examples of how to format a variety of sources. If you have a reference source for which you are not able to find the correct APA format, contact me for help anytime (philipw@bgsu.edu). Keep in mind that an incorrectly formatted manuscript will be returned to you, a delay that may cause it to be moved to a subsequent issue of the journal.

1. Word document page setup: Top = 1", Bottom = 1", Left = 1.25", Right = 1.25". This is the default setting for Microsoft Word.
2. Page breaks, tabs, and indents: Do not use page breaks or tabs. Do not use spaces for paragraph indents; use the scroll markers, as shown here. 
3. Paper title: Centered at the top of the first page with a 22-point Times New Roman (Bold), Small-Caps font.
4. Body fonts: Use 10-point Times New Roman (TNR) for body text throughout (1/8" paragraph indentation); 9-point TNR for author names/affiliations under the paper title; 16-point TNR for major section titles; 14-point TNR for minor section titles; 9-point TNR BOLD for caption titles; other font sizes may be noted in the sample Word document.
5. Images: All images should be included in the body of the document. It's ok for images or tables to be centered on the page, and not confined to the 2-column format, if necessary. Irrespective of how Word moves any given image/table, be certain that all captions are located in the document where the images/tables should ultimately be placed. If you are required to submit additional high-quality images, they must be saved/sent as individual files (one image per file) and labeled using the following format, where the first portion of the title is your manuscript number:
J17-F-09 Figure 7
6. In-text referencing: List and number each reference when referring to them in the body of the document (e.g., [1]). In-text references must be in numerical order and follow entries in the References section. Again, see the sample Word document on our website for specifics. Please do not use the End-Page Reference utility in Microsoft Word.
7. Tables and figures: Captions for tables must be above the table, while captions for figures are below; all captions are left-justified unless the table or figure is centered on the page, in which case the caption should also be centered.
8. Page limit: Manuscripts should not be more than 15 pages (single-spaced, 2-column format).
9. Page numbering: Do not use page numbers.